

ENGO 697

Remote Sensing Systems and Advanced Analytics

Session 8: How to solve key hyper-/multi-spectral radiative transfer models (RTM)

Dr. Linlin (Lincoln) Xu

Linlin.xu@ucalgary.ca

Office: ENE 221

Key Canopy RTMs

- (1) **PROSPECT Model:** Describe leaf reflectance and transmittance spectrum as a function of some **biochemical** parameters, e.g., chlorophyll content and water content in leaves;
- (1) **SAIL Model:** Describe canopy reflectance spectrum as a function of some **biophysical/structural** parameters of canopy, e.g., LAI, solar angle;
- (1) **PROSAIL Model:** PROSAIL = POSPECT + SAIL, a function of both **biochemical** and **biophysical/structural** parameters of leaves and canopy;

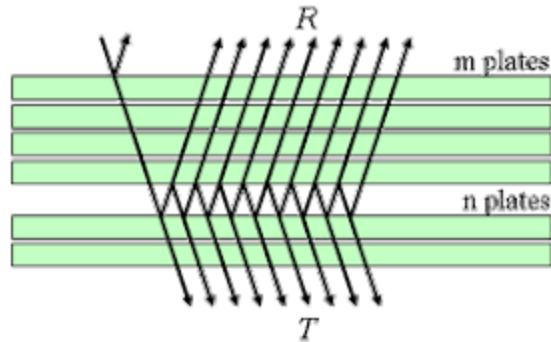
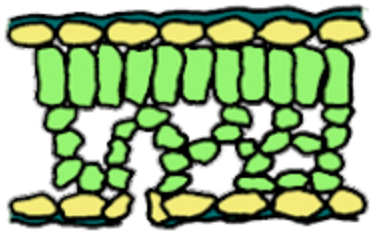
Prospect Model (Allen et al. 1969, Jacquemoud and Barret, 1990)



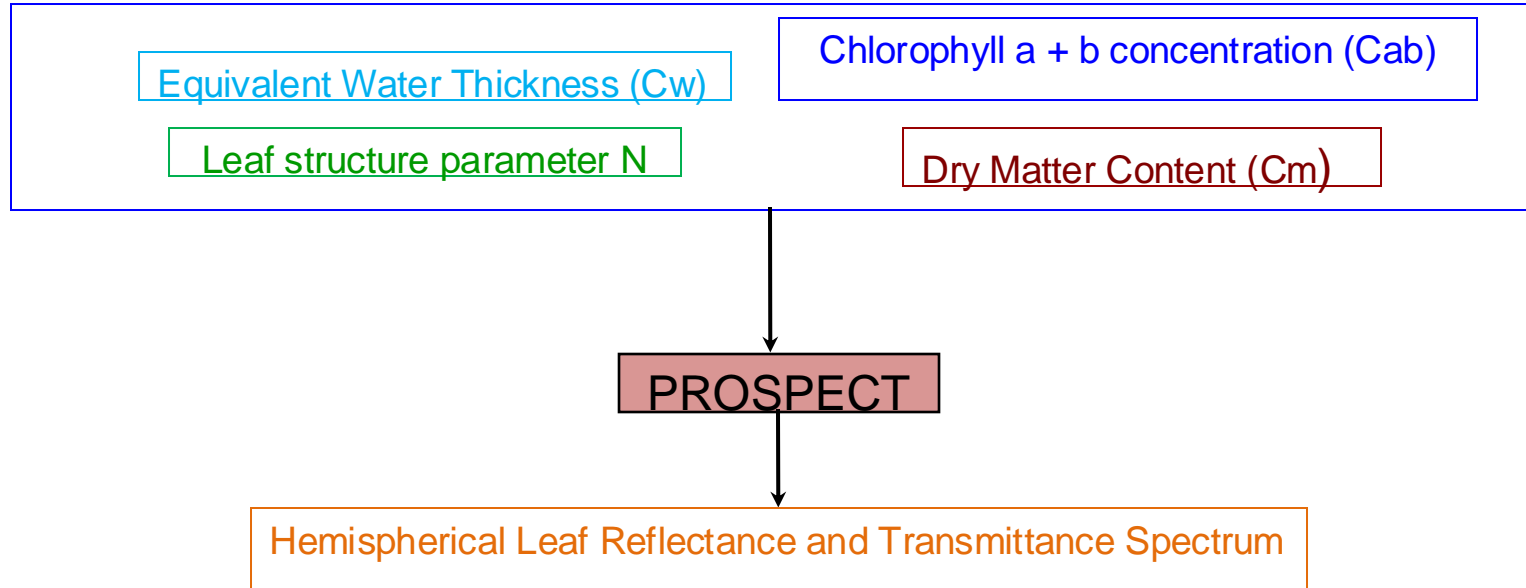
(1) Prospect is a **leaf-level RTM** that describes the **transmittance and reflectance characteristics** (400nm to 2500nm) of leaves as a function of some leaf biochemical parameters, i.e.,

Leaf structure parameter N ,
chlorophyll a + b concentration (C_{ab}) ($\mu\text{g}/\text{cm}^2$),
equivalent water thickness (C_w) (cm), and
dry matter content (C_m) (g/cm^2).

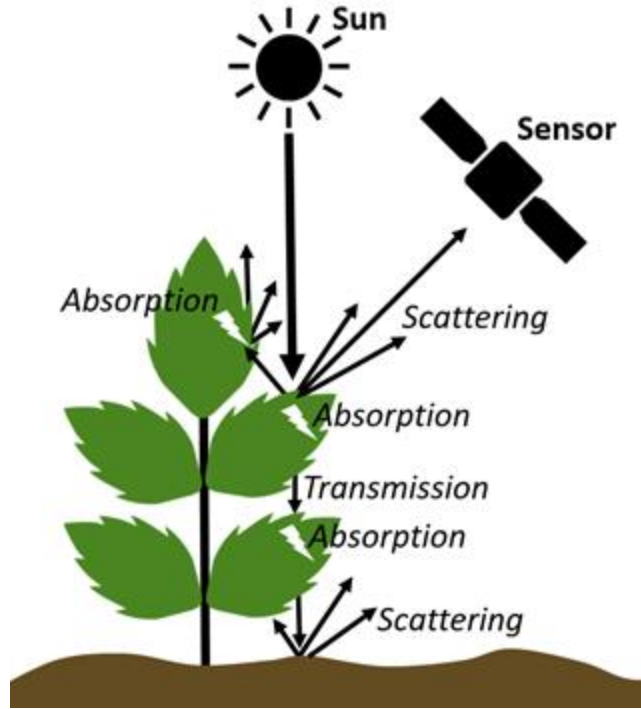
(2) Prospect represents leaf as one or a stack of several **absorbing plates** with rough surfaces (equivalent to isotropic scattering).
http://photobiology.info/Jacq_Ustin.html



PROSPECT:



Sail Model (W. VERHOEF, 1984, 1985)



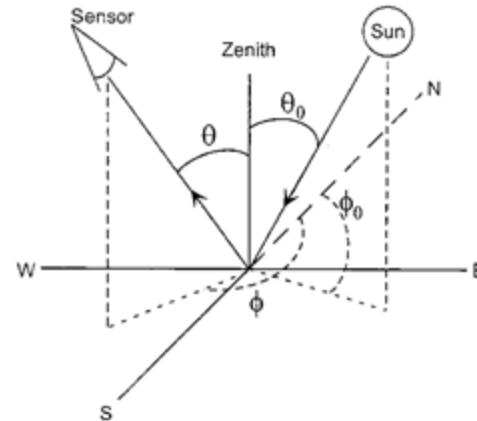
Radiative transfer in plant canopies, i.e. transmission, absorption and scattering (Kattenborn, 2018)

(1) Sail is a **Canopy-level RTM** that describes the **reflectance characteristics** (400nm to 2500nm) of Canopy as a function of some biophysical and geometric parameters, i.e.,

Canopy structural parameters (i.e., Leaf Inclination Angle and LAI)

Soil spectral reflectance,

Illumination and acquisition geometry (i.e., Zenith Solar Angle, Zenith and Relative Azimuth angles) and Fraction of Diffuse Illumination (skyl, also called an atmospheric parameter)



Sail:

Canopy Parameters:

LAI

Leaf Inclination Angle (θ_l)

View & Illumination Parameter:

Zenith and Relative Azimuth angles (θ_v, ψ_v)

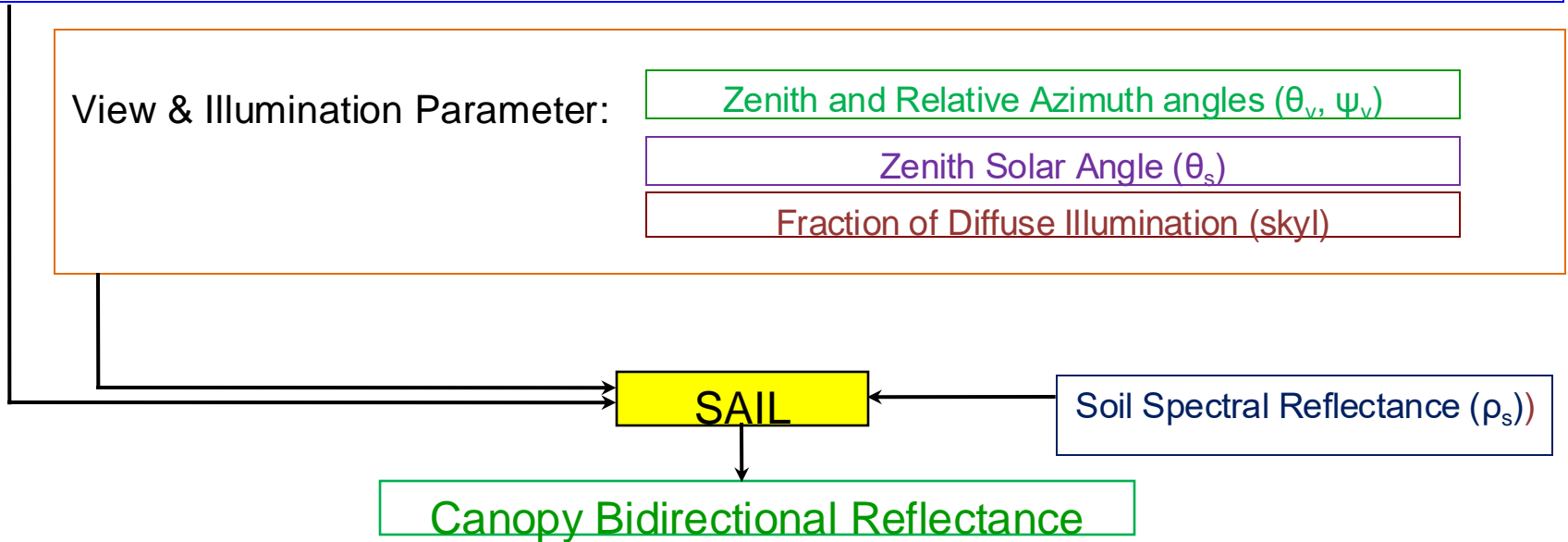
Zenith Solar Angle (θ_s)

Fraction of Diffuse Illumination (skyl)

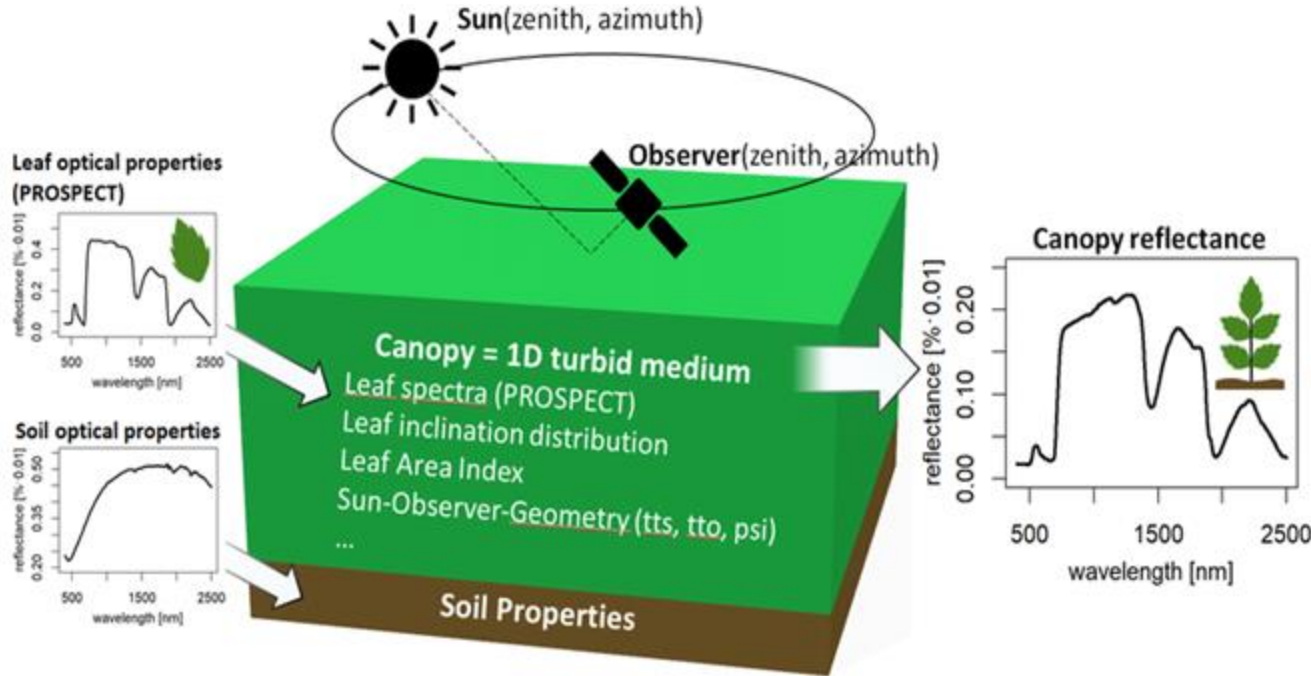
SAIL

Soil Spectral Reflectance (ρ_s)

Canopy Bidirectional Reflectance



Prosail = Prospect + Sail (Verhoef et al. 2007)

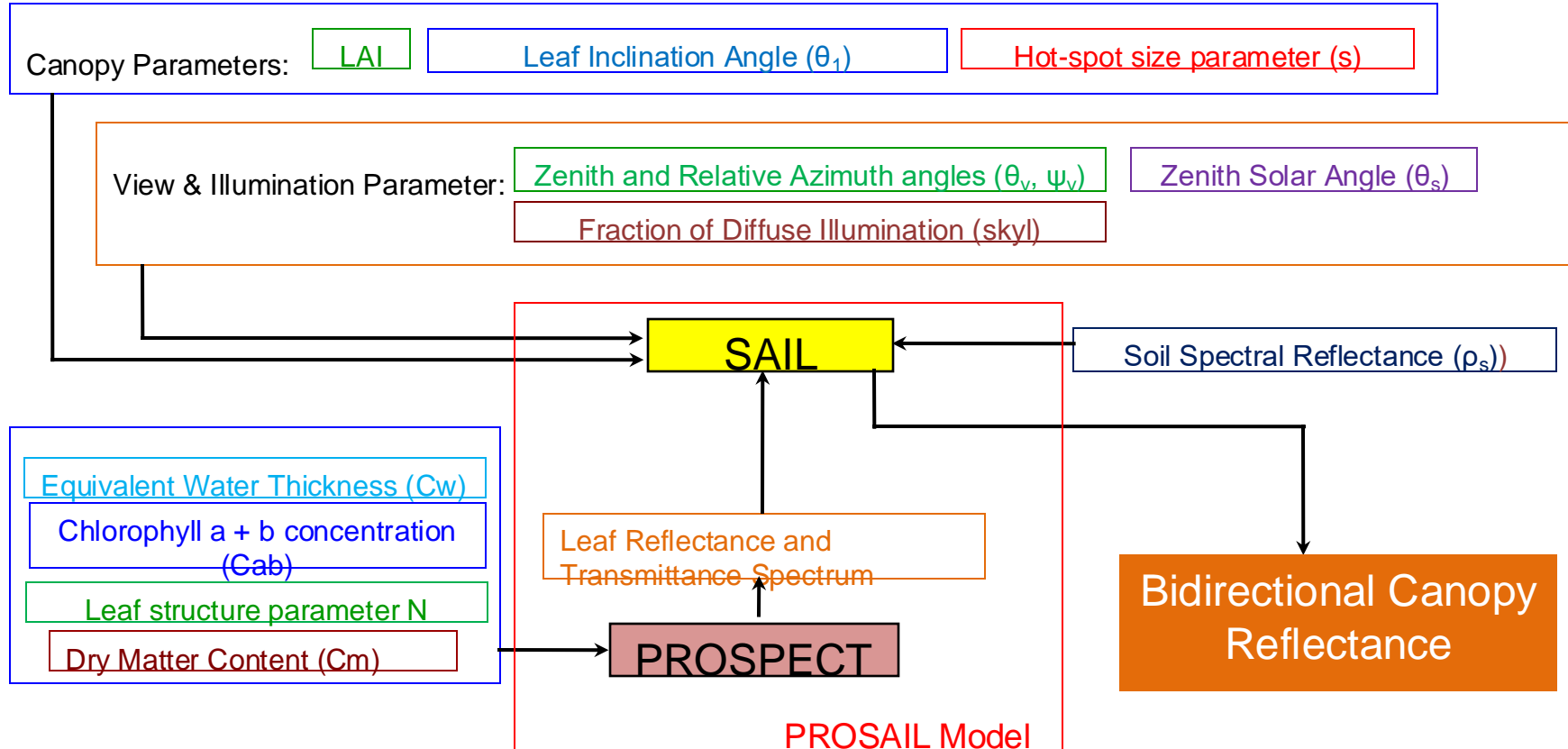


(1) Prosail integrates Prospect into Sail to link **Canopy-level RTM** with **leaf-level RTM**;

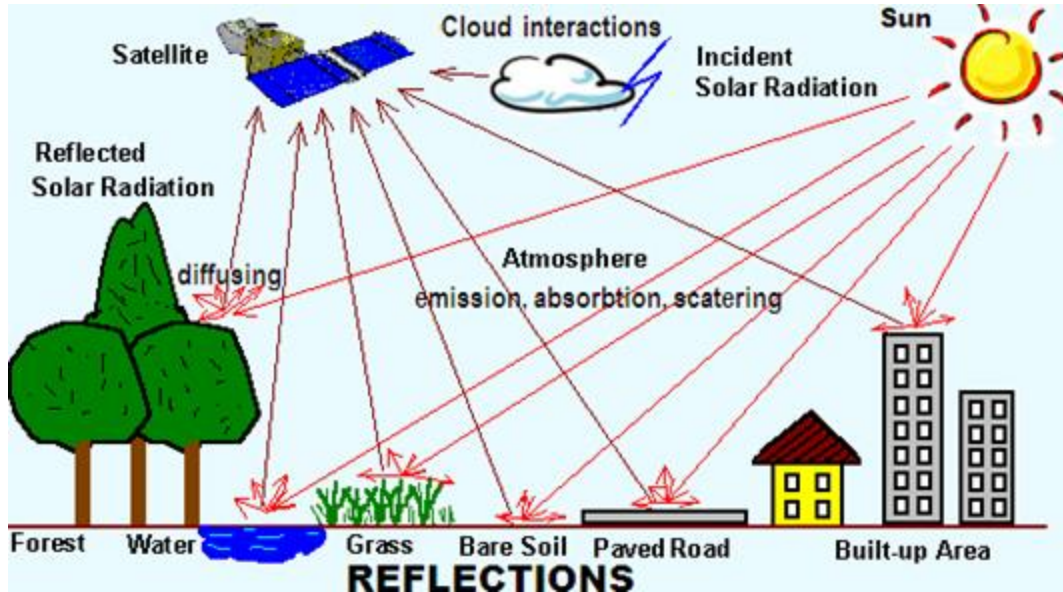
(2) Prosail has 14 input parameters, including **both biochemical and biophysical parameters**;

(3) Prosail outputs the bidirectional reflectance of canopy, from 400 to 2500 nm in 1 nm increments.

Prosail = Prospect + Sail



Remote Sensing System Overview



Forward model:

$$Y = f(X)$$

(1) Y: received radiation by the sensor

(2) X: variables that you want to know, e.g., class labels, chlorophyll content in leaves, leaf area index/density;

Inverse model:

$$X = g(Y, \theta)$$

where $g(\cdot)$ is an **unknown** inverse function with **unknown** model parameter θ .

Why estimating X is difficult?

--- Knowledge $f(\cdot)$ complex, biased, highly nonlinear, with large uncertainty;



---- Data (X, Y) pairs limited, poor quality;

---- Prior information (e.g., spatial prior) ambiguous;

	(1) Direct inversion	(2) LUT approach	(3) Numerical Approach	(4) Simulation & ML	(5) ML	(6) DL
$f(\cdot)$ is known	yes	yes	yes	yes	yes	yes
$f(\cdot)$ is partially known, i.e., form known, but with some unknown parameters U	no	no	Yes, estimate X and U together	no	no	no
$f(\cdot)$ unknown, (X,Y) known	no	no	no	no	yes	yes
$f(\cdot)$ unknown, (X,Y) unknown	no	no	no	no	no	no
If both $f(\cdot)$ and (X,Y) known, can accommodate both?	no	yes?	Yes? Use (X,Y) to estimate parameters in $f(\cdot)$	yes?	Yes, use both simulated and observed data	Yes, use both simulated and observed data
Can use prior information ? e.g., spatial prior and value prior	no	Yes? Use value prior for sampling	Yes? Use value prior of X in Bayesian estimation	Yes, Use value prior in sampling and spatial prior in Random fields	Yes, spatial prior in Random field approaches	Yes, similar to ML
Advantages	Knowledge-driven; Simple, easy	Knowledge-driven; Intuitive, easy, discrete fitting;	Knowledge-driven; estimate U; Efficient for simple $f(\cdot)$ in convex problems	Knowledge-driven; flexible; continuous fitting; good inter/extrapolation; faster than LUT	Data-driven; flexible; Classic;	Strong modeling capability; automatic feature learning;
Disadvantages	Unrealistic; rely on simple $f(\cdot)$	Sensitive to accuracy of $f(\cdot)$, similarity metrics, sampling density and range; slow if LUT is large; bad for extrapolation;	Rely on efficiency of nonlinear solver; Slow; Local optimum;	Overfitting and underfitting risk to simulated data; difficult model selection; Sensitive to accuracy of $f(\cdot)$, similarity metrics, sampling density and range;	Weak modeling capability; Rely on "good" engineered features; Black-box; Overfitting, underfitting; Feature and model selection is difficult and slow	Overfitting and underfitting; Black-box;

Review

Evaluation of the PROSAIL Model Capabilities for Future Hyperspectral Model Environments: A Review Study

Katja Berger ^{1,*}, Clement Atzberger ², Martin Danner ¹ , Guido D'Urso ³ , Wolfram Mauser ¹, Francesco Vuolo ² and Tobias Hank ¹

¹ Department of Geography, Ludwig-Maximilians-Universität München, Luisenstraße 37, D-80333 Munich, Germany; martin.danner@iggf.geo.uni-muenchen.de (M.D.); w.mauser@lmu.de (W.M.); tobias.hank@lmu.de (T.H.)

² Institute of Surveying, Remote Sensing & Land Information (IVFL), University of Natural Resources and Life Sciences, Vienna (BOKU), Peter Jordan Str. 82, 1190 Vienna, Austria; clement.atzberger@boku.ac.at (C.A.); francesco.vuolo@boku.ac.at (F.V.)

³ Department of Agricultural Engineering and Agronomy, University of Naples Federico II, Via Università 100, 80055 Portici (Na), Italy; durso@unina.it

* Correspondence: katja.berger@lmu.de; Tel.: +49-89-2180-6695

Received: 24 November 2017; Accepted: 8 January 2018; Published: 10 January 2018

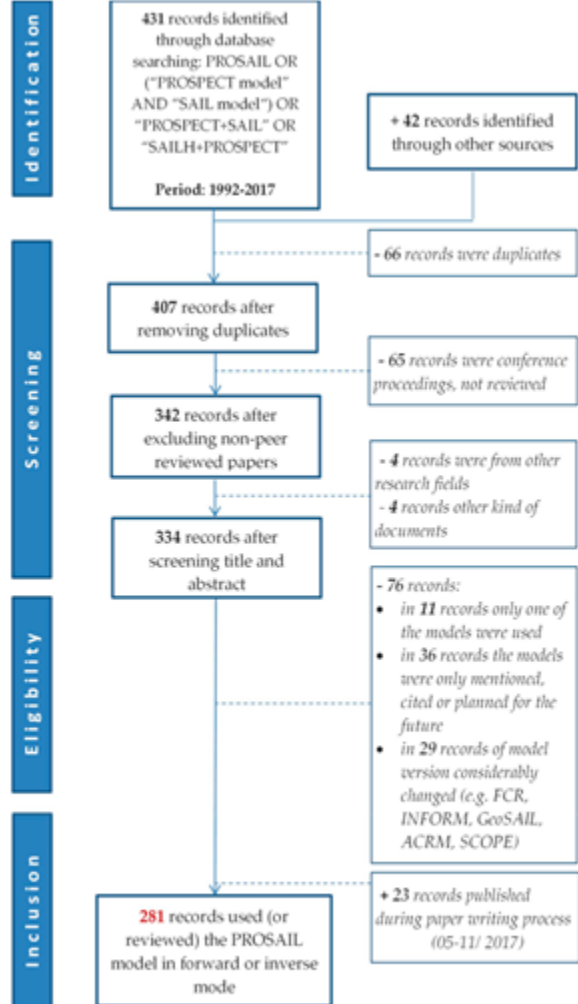


Figure 2. Systematic literature review flow chart.

8. Variable Retrieval Methods

Researchers, who used the PROSAIL model for biophysical and biochemical variable retrieval, applied the following approaches:

- parametric: indirect use of the model by building an arithmetic combination of two or more bands (=simple ratio or orthogonal VIs) and relating it to the variable of interest (these parametric models are then applied to real data, see also introduction);
- radiometric-data driven (i): numerical iterative optimization techniques;
- radiometric-data driven (ii): look-up tables (LUTs);
- hybrid methods: combining a non-linear, non-parametric statistical approach with the physically based PROSAIL model. (i): ANNs and (ii): other machine learning regression algorithms, such as GPR or SVM.

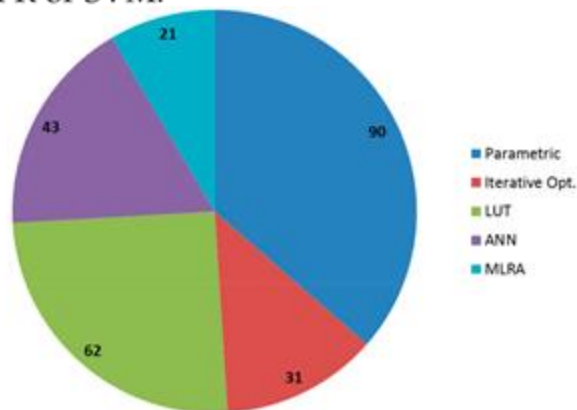


Figure 6. Variable retrieval methods of all evaluated studies involving the PROSAIL model. Parametric regression refers to vegetation indices. The absolute number of studies using the respective algorithm is indicated.

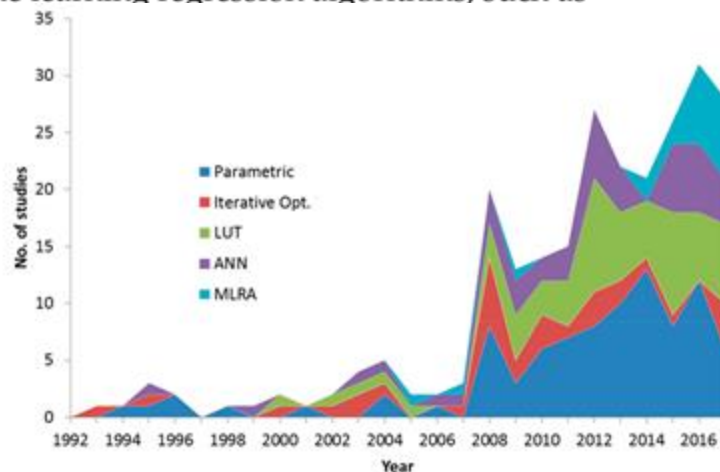


Figure 7. Temporal development of applications of different variable retrieval methods involving the PROSAIL model from 1992 to 2017.

(a) Parametric Approach

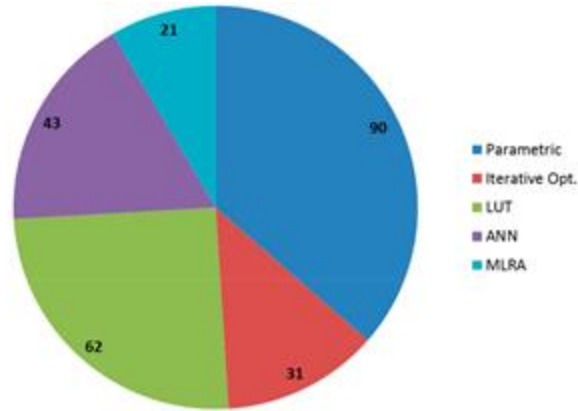


Figure 6. Variable retrieval methods of all evaluated studies involving the PROSAIL model. Parametric regression refers to vegetation indices. The absolute number of studies using the respective algorithm is indicated.

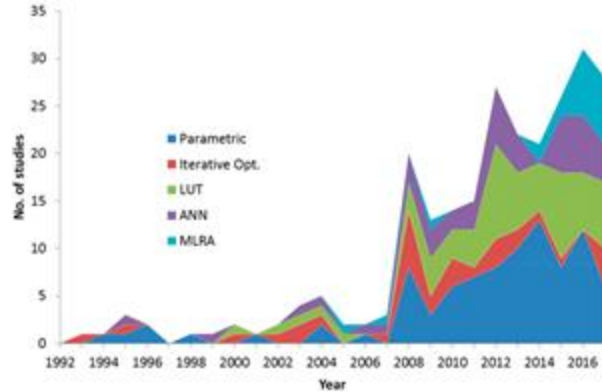


Figure 7. Temporal development of applications of different variable retrieval methods involving the PROSAIL model from 1992 to 2017.

Based on Forward model $Y = f(X)$:

Step 1: Use Prosail model to simulate (X_i, Y_i) pairs;

Step 2: Extracted **vegetation indices (VI)** from $\{Y_i\}$, and build (X_i, VI_i) pairs;

Step 3: Build linear regression model $X=g(VI)$, e.g., $X_i=a*VI1+b*VI2+c$, estimate parameters $\theta=\{a,b,c\}$, by $J(\theta) = \sum ||X_i-g(VI)||$, $\theta = \min J(\theta)$

Step 4: Once θ is known, given $Y \rightarrow VI$, use $X=g(VI)$ to estimate X

Popularity and Trend:

Very popular. More than **one third** of all studies use this approach, as shown in Fig. 6. But, it has a **decreasing tendency**, as indicated by Figure 7.

Advantages:

Low calculation complexity, high computation power and speed, while still delivering meaningful results, e.g., Broge et al. 2000. Popular VIs includes ratio vegetation index (RVI) and normalized difference vegetation index (NDVI),

Disadvantages:

(1) **Lack of novelty**, because VI have been exhaustively exploited. (2) VI has **low transferability**. (3) VIs make only **limited use of the full spectral resolution** available. (4) essentially **knowledge-driven feature engineering**, so difficult to determine the “best” feature subset from all available VIs.

	(1) Direct inversion	(2) LUT approach	(3) Numerical Approach	(4) Simulation & ML	(5) ML	(6) DL
$f(\cdot)$ is known	yes	yes	yes	yes	yes	yes
$f(\cdot)$ is partially known, i.e., form known, but with some unknown parameters U	no	no	Yes, estimate X and U together	no	no	no
$f(\cdot)$ unknown, (X,Y) known	no	no	no	no	yes	yes
$f(\cdot)$ unknown, (X,Y) unknown	no	no	no	no	no	no
If both $f(\cdot)$ and (X,Y) known, can accommodate both?	no	yes?	Yes? Use (X,Y) to estimate parameters in $f(\cdot)$	yes?	Yes, use both simulated and observed data	Yes, use both simulated and observed data
Can use prior information ? e.g., spatial prior and value prior	no	Yes? Use value prior for sampling	Yes? Use value prior of X in Bayesian estimation	Yes, Use value prior in sampling and spatial prior in Random fields	Yes, spatial prior in Random field approaches	Yes, similar to ML
Advantages	Knowledge-driven; Simple, easy	Knowledge-driven; Intuitive, easy, discrete fitting;	Knowledge-driven; estimate U; Efficient for simple $f(\cdot)$ in convex problems	Knowledge-driven; flexible; continuous fitting; good inter/extrapolation; faster than LUT	Data-driven; flexible; Classic;	Strong modeling capability; automatic feature learning;
Disadvantages	Unrealistic; rely on simple $f(\cdot)$	Sensitive to accuracy of $f(\cdot)$, similarity metrics, sampling density and range; slow if LUT is large; bad for extrapolation;	Rely on efficiency of nonlinear solver; Slow; Local optimum;	Overfitting and underfitting risk to simulated data; difficult model selection; Sensitive to accuracy of $f(\cdot)$, similarity metrics, sampling density and range;	Weak modeling capability; Rely on "good" engineered features; Black-box; Overfitting, underfitting; Feature and model selection is difficult and slow	Overfitting and underfitting; Black-box;

(4) Data Simulation & Machine Learning (ML) Approaches

If the radiative transfer model $f(\cdot)$ is known, we can simulate a collection of X and Y pairs, i.e., $\{(X_j, Y_j) \mid j=1,2,\dots,M\}$. Instead of using LUT for data inversion, we can use ML approaches to learn the inverse function, i.e., $X=g(Y)$, and use this inverse function to estimate the X value of an observed Y value.

Forward model: $Y = f(X)$, where $f(\cdot)$ is the radiative transfer models, which tend to be highly nonlinear and not invertible.

Based on $Y=f(X)$, similar to LUT, we simulate the following X and Y pairs.

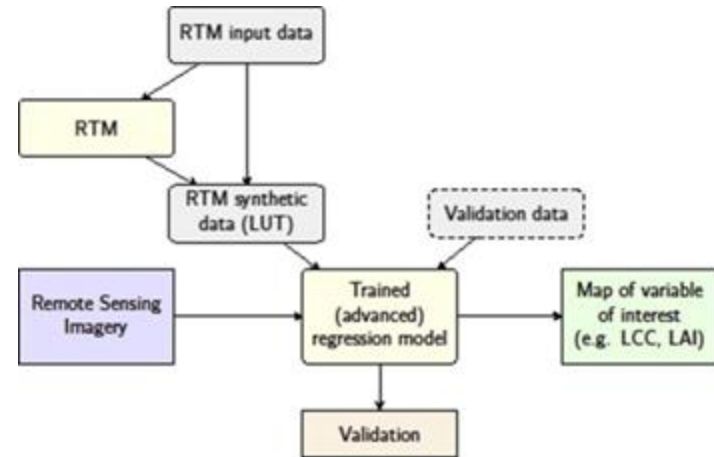
X_1 : Y_1
 X_2 : Y_2
 X_3 : Y_3
.....
 X_4 : Y_4

Based on simulated $\{(X_j, Y_j) \mid j=1,2,\dots,M\}$ pairs, we build the following objective function:

$$J(\theta) = \sum \|X_i - g(Y_i)\|$$
$$\theta = \min J(\theta)$$

where θ is the unknown parameters in the inverse function $g(\cdot)$ which is a statistical model or machine learning model. Once we know θ , we can establish the inverse function $g(\cdot)$, and use it to estimate the X value of an observed Y value by $X=g(Y)$.

Comparing with the LUT approach that is essentially discrete interpolation, the ML approaches can learn a continuous inverse function $g(\cdot)$ using the simulated data, and thereby they theoretically can achieve more accurate estimation. Moreover, ML approaches tend to be faster because they do not need to do LUT searching for every observation.



(b) Numerical Iterative Optimization Approach

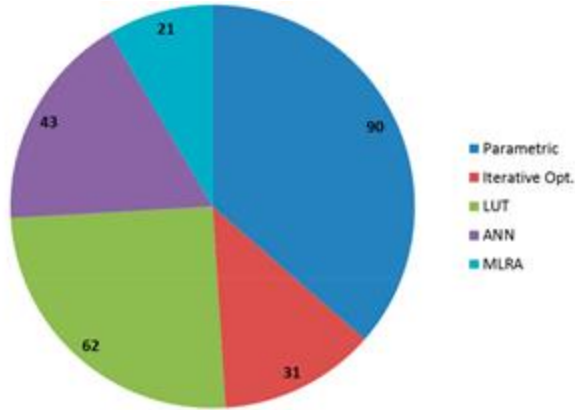


Figure 6. Variable retrieval methods of all evaluated studies involving the PROSAIL model. Parametric regression refers to vegetation indices. The absolute number of studies using the respective algorithm is indicated.

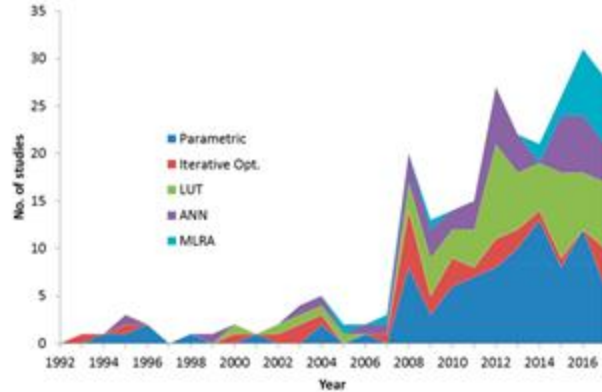


Figure 7. Temporal development of applications of different variable retrieval methods involving the PROSAIL model from 1992 to 2017.

Based on Forward model $Y = f(X)$ and a spectra observation Y_i

Step 1: Build an objective function $J(X_i) = \|Y_i - f(X_i)\|$

Step 2: Estimate X_i by $X_i = \min J(X_i)$ using iterative nonlinear optimization approaches, e.g., gradient descent, Markov chain monte carlo (MCMC), etc.

Popularity and Trend:

Not popular and decreasing trend (Bicheron and Loroy, 1999; Goel and Thompson, 1984)

Advantages:

Does not need data simulation based on forward model;

Can directly estimate X_i given spectra observation Y_i ;

Disadvantages:

- (1) high computational loads;
- (2) high risk of converging to local minima;

	(1) Direct inversion	(2) LUT approach	(3) Numerical Approach	(4) Simulation & ML	(5) ML	(6) DL
$f(\cdot)$ is known	yes	yes	yes	yes	yes	yes
$f(\cdot)$ is partially known, i.e., form known, but with some unknown parameters U	no	no	Yes, estimate X and U together	no	no	no
$f(\cdot)$ unknown, (X,Y) known	no	no	no	no	yes	yes
$f(\cdot)$ unknown, (X,Y) unknown	no	no	no	no	no	no
If both $f(\cdot)$ and (X,Y) known, can accommodate both?	no	yes?	Yes? Use (X,Y) to estimate parameters in $f(\cdot)$	yes?	Yes, use both simulated and observed data	Yes, use both simulated and observed data
Can use prior information ? e.g., spatial prior and value prior	no	Yes? Use value prior for sampling	Yes? Use value prior of X in Bayesian estimation	Yes, Use value prior in sampling and spatial prior in Random fields	Yes, spatial prior in Random field approaches	Yes, similar to ML
Advantages	Knowledge-driven; Simple, easy	Knowledge-driven; Intuitive, easy, discrete fitting;	Knowledge-driven; estimate U; Efficient for simple $f(\cdot)$ in convex problems	Knowledge-driven; flexible; continuous fitting; good inter/extrapolation; faster than LUT	Data-driven; flexible; Classic;	Strong modeling capability; automatic feature learning;
Disadvantages	Unrealistic; rely on simple $f(\cdot)$	Sensitive to accuracy of $f(\cdot)$, similarity metrics, sampling density and range; slow if LUT is large; bad for extrapolation;	Rely on efficiency of nonlinear solver; Slow; Local optimum;	Overfitting and underfitting risk to simulated data; difficult model selection; Sensitive to accuracy of $f(\cdot)$, similarity metrics, sampling density and range;	Weak modeling capability; Rely on "good" engineered features; Black-box; Overfitting, underfitting; Feature and model selection is difficult and slow	Overfitting and underfitting; Black-box;

(2) Numerical Approaches

If the radiative transfer model $f(\cdot)$ is known, and we have an remote sensing observation Y , we can use the numerical approach to estimate the associated X .

Forward model: $Y = f(X)$, where $f(\cdot)$ is the radiative transfer models, which tend to be highly nonlinear and un-invertible.

Based on some observations $\{Y\}$, we can build an objective function:

$$J(X) = Y - f(X)$$

$$X = \min J(X)$$

We try to find X that through $f(\cdot)$ can generate output whose value is very close to the value of Y .

There are many methods that can solve this nonlinear optimization problems, for example,

---- Newton's method

---- Gradient descent methods

---- Simulated annealing approach

Because the forward model $f(\cdot)$ contains knowledge and physical rules, $f(\cdot)$ is usually called physical model.

(c) LUT Approach

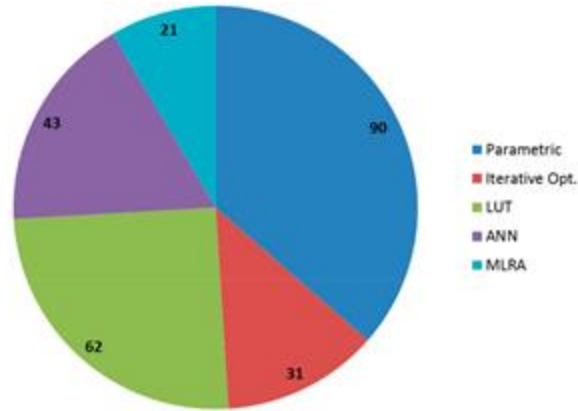


Figure 6. Variable retrieval methods of all evaluated studies involving the PROSAIL model. Parametric regression refers to vegetation indices. The absolute number of studies using the respective algorithm is indicated.

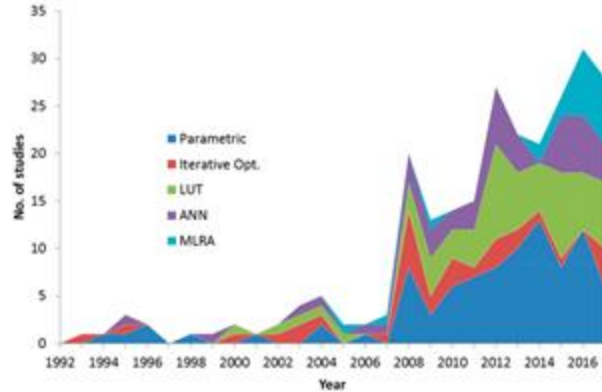


Figure 7. Temporal development of applications of different variable retrieval methods involving the PROSAIL model from 1992 to 2017.

Based on Forward model $Y = f(X)$:

Step 1: Use Prosail model to **simulate** (X_i, Y_j) pairs and **build a LUT**;

Step 2: Given an observed Y value, we **search the LUT** to identify the row whose Y_j value is the closest to the observed Y value.

Step 3: The X_j value **associated with Y_j** is treated as the estimated X value of Y .

Popularity and Trend:

Extensively used in the last decades; Combal et al., 2002; Knyazikhin et al, 1998; Weiss et al., 2000

Increasing trend, as indicated by Figure 7.

Advantages:

Much faster than iterative optimization approach;

Provide possibility to **overcome the problem of local optima**;

Allow the **integration of prior information** into the building of LUT;

Disadvantages:

(1) **searching algorithm is computationally inefficient**, especially when the number of spectral channels is high; (2) a **discrete optimization approach, cannot perform accurate interpolation and extrapolation**;

	(1) Direct inversion	(2) LUT approach	(3) Numerical Approach	(4) Simulation & ML	(5) ML	(6) DL
$f(\cdot)$ is known	yes	yes	yes	yes	yes	yes
$f(\cdot)$ is partially known, i.e., form known, but with some unknown parameters U	no	no	Yes, estimate X and U together	no	no	no
$f(\cdot)$ unknown, (X,Y) known	no	no	no	no	yes	yes
$f(\cdot)$ unknown, (X,Y) unknown	no	no	no	no	no	no
If both $f(\cdot)$ and (X,Y) known, can accommodate both?	no	yes?	Yes? Use (X,Y) to estimate parameters in $f(\cdot)$	yes?	Yes, use both simulated and observed data	Yes, use both simulated and observed data
Can use prior information ? e.g., spatial prior and value prior	no	Yes? Use value prior for sampling	Yes? Use value prior of X in Bayesian estimation	Yes, Use value prior in sampling and spatial prior in Random fields	Yes, spatial prior in Random field approaches	Yes, similar to ML
Advantages	Knowledge-driven; Simple, easy	Knowledge-driven; Intuitive, easy, discrete fitting;	Knowledge-driven; estimate U; Efficient for simple $f(\cdot)$ in convex problems	Knowledge-driven; flexible; continuous fitting; good inter/extrapolation; faster than LUT	Data-driven; flexible; Classic;	Strong modeling capability; automatic feature learning;
Disadvantages	Unrealistic; rely on simple $f(\cdot)$	Sensitive to accuracy of $f(\cdot)$, similarity metrics, sampling density and range; slow if LUT is large; bad for extrapolation;	Rely on efficiency of nonlinear solver; Slow; Local optimum;	Overfitting and underfitting risk to simulated data; difficult model selection; Sensitive to accuracy of $f(\cdot)$, similarity metrics, sampling density and range;	Weak modeling capability; Rely on "good" engineered features; Black-box; Overfitting, underfitting; Feature and model selection is difficult and slow	Overfitting and underfitting; Black-box;

(3) LookUp Table (LUT) Approaches

If the radiative transfer model $f(\cdot)$ is known, we can simulate a collection of X and Y pairs, i.e., $\{(X_j, Y_j) \mid j=1,2,\dots,M\}$, based on which we can build a LUT and use it to estimate the X value of an observed Y value.

Forward model: $Y = f(X)$, where $f(\cdot)$ is the radiative transfer models, which tend to be highly nonlinear and not invertible.

Based on $Y=f(X)$, we build a LUT by first sampling X_j uniformly within a range $[A,B]$ (A and B are respectively the theoretical min and max value of X), and then obtaining the associated Y_j value by $Y_j=f(X_j)$.

X_1	:	Y_1
X_2	:	Y_2
X_3	:	Y_3
....		
X_4	:	Y_4

Given an observed Y value, how do we estimate its X value using LUT? First, we search the LUT to identify the row whose Y_j value is the closest to the observed Y value. Then, the X_j value associated with Y_j is treated as the estimated X value of Y .

Comparing with the numerical approaches, the LUT approach is simpler and has theoretical advantages such as being able to find the global optimum in the parameter space, and thereby the LUT approaches have been widely used in solving remote sensing inverse problems.

(d) Machine Learning Regression Algorithm (MLRA)

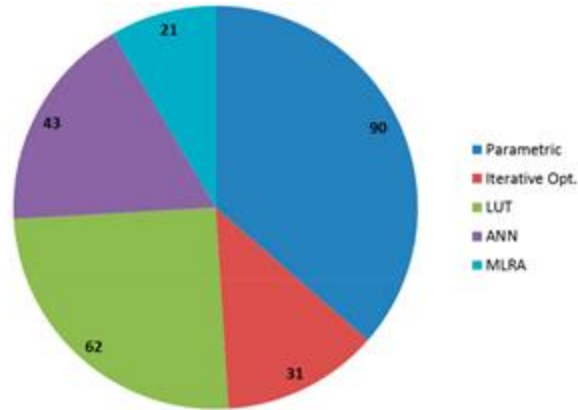


Figure 6. Variable retrieval methods of all evaluated studies involving the PROSAIL model. Parametric regression refers to vegetation indices. The absolute number of studies using the respective algorithm is indicated.

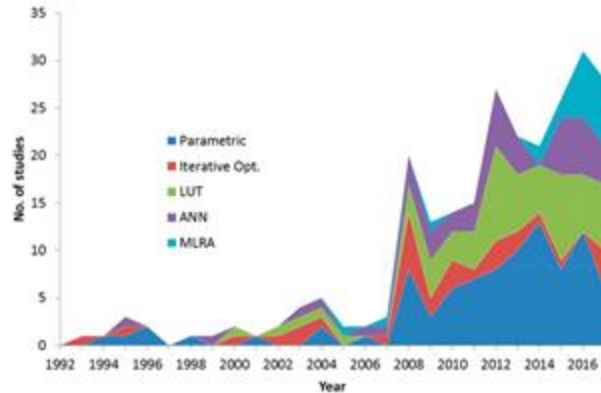


Figure 7. Temporal development of applications of different variable retrieval methods involving the PROSAIL model from 1992 to 2017.

Based on Forward model $Y = f(X)$:

Step 1: Use Prosail model to simulate (X_i, Y_i) pairs;

Step 2: Build nonlinear regression model $X=g(Y_i)$, e.g., ANN, SVR, Gaussian process regression (GPR), by $J(\theta) = \sum ||X_i - g(Y_i)||$, $\theta = \min J(\theta)$

Step 3: Once θ is known, given Y , use $X=g(Y)$ to estimate X

Popularity and Trend:

Very popular (ANN + MLRA) in Fig. 6; Fast growing trend (ANN + MLRA) in Fig. 7;

Advantages:

Comparing with (a) parametric approach, (d) is **nonlinear**, **uses all spectral channels** and does not need to extract VIs as model input;

Comparing with (c) LUT approach, (d) **allows continuous interpolation and extrapolation**;

Disadvantages:

Low model complexity comparing with deep neural networks;

Relies on feature engineering to generate discriminative spatial-spectral features;

	(1) Direct inversion	(2) LUT approach	(3) Numerical Approach	(4) Simulation & ML	(5) ML	(6) DL
$f(\cdot)$ is known	yes	yes	yes	yes	yes	yes
$f(\cdot)$ is partially known, i.e., form known, but with some unknown parameters U	no	no	Yes, estimate X and U together	no	no	no
$f(\cdot)$ unknown, (X,Y) known	no	no	no	no	yes	yes
$f(\cdot)$ unknown, (X,Y) unknown	no	no	no	no	no	no
If both $f(\cdot)$ and (X,Y) known, can accommodate both?	no	yes?	Yes? Use (X,Y) to estimate parameters in $f(\cdot)$	yes?	Yes, use both simulated and observed data	Yes, use both simulated and observed data
Can use prior information ? e.g., spatial prior and value prior	no	Yes? Use value prior for sampling	Yes? Use value prior of X in Bayesian estimation	Yes, Use value prior in sampling and spatial prior in Random fields	Yes, spatial prior in Random field approaches	Yes, similar to ML
Advantages	Knowledge-driven; Simple, easy	Knowledge-driven; Intuitive, easy, discrete fitting;	Knowledge-driven; estimate U; Efficient for simple $f(\cdot)$ in convex problems	Knowledge-driven; flexible; continuous fitting; good inter/extrapolation; faster than LUT	Data-driven; flexible; Classic;	Strong modeling capability; automatic feature learning;
Disadvantages	Unrealistic; rely on simple $f(\cdot)$	Sensitive to accuracy of $f(\cdot)$, similarity metrics, sampling density and range; slow if LUT is large; bad for extrapolation;	Rely on efficiency of nonlinear solver; Slow; Local optimum;	Overfitting and underfitting risk to simulated data; difficult model selection; Sensitive to accuracy of $f(\cdot)$, similarity metrics, sampling density and range;	Weak modeling capability; Rely on "good" engineered features; Black-box; Overfitting, underfitting; Feature and model selection is difficult and slow	Overfitting and underfitting; Black-box;

Deep learning in vegetation remote sensing

Concerning biochemical and structural plant traits, an interesting approach is to **train CNNs with simulated data derived from physically based models**. Such hybrid approaches, i.e. coupling statistical and process-based models, may not only provide data for training but also enable including priors and realistic constraints in model training (Reichstein et al., 2019).

For instance, Annala et al. (2020) trained a **1DCNN** with reflectance spectra simulated with the radiative transfer model (RTM) **SLOP** (Maier et al., 1999). Although SLOP is a relatively simple leaf reflectance model, Annala et al. (2020) demonstrated promising tests of this hybrid inversion method for UAV hyperspectral acquisitions of forest canopies. More sophisticated RTMs may allow to produce more robust models, e.g. PROSAIL (Jacquemoud et al., 2009), enabling to account for bidirectional reflectance effects in plant canopies, whereas **3D-RTMs such as FLIGHT** (North, 1996) or DART (Gastellu-Etchegorry et al., 1996) may provide interesting sources for generating synthetic training data for **2D-CNNs** (see Section 3.2 for details on 1D-, 2D- and 3D-CNNs).

Kattenborn, T., Leitloff, J., Schiefer, F., & Hinz, S. (2021). Review on Convolutional Neural Networks (CNN) in vegetation remote sensing. *ISPRS Journal of Photogrammetry and Remote Sensing*, 173, 24-49.

Reichstein, M., Camps-Valls, G., Stevens, B., Jung, M., Denzler, J., Car-valhais, N., Prabhat, 2019. **Deep learning and process understanding for data-driven Earth system science**. *Nature* 566 (7743), 195–204. <https://doi.org/10.1038/s41586-019-0912-1> (cit. on pp. 6, 22, 24, 57, 60).

Deep Learning (DL) for Inverting Prosail Model

(1) Use DL as a regression technique to directly obtain the inverse function $X=g(Y)$ based on simulations from the Prosail model;

(2) Use DL as an unsupervised feature extraction approach to learn efficient features, which can be used boost the LUT approach;

LUT Inversion of PROSAIL using Hyperspectral Imagery

Advantages:

- The possibility for obtaining **global optima** in the parameter space;
- Strong model **transferability**;
- Good accuracy and precision**;

Disadvantages:

- Large **computational cost** due to high-dimensionality and spectral redundancy;
- Difficult to define a similarity measure** for high-dimensional hyperspectral data;

Current Dimensionality reduction approaches:

- Knowledge-driven** feature engineering approach, e.g., vegetation indices;
- Difficult to select subset** of features from all possible features;

Feature Engineering vs. Feature Learning

- Feature Engineering

- Knowledge-driven, requires knowing what makes “good” features;

- Does not handle data variability very well;

- Requires feature selection from many possible features;

- Lower accuracy in computer vision and machine learning applications;

- Feature Learning:

- Data-driven, relies on the data to obtain meaningful features;

- Can well adapt to the characteristics of the data;

- Does not require feature selection;

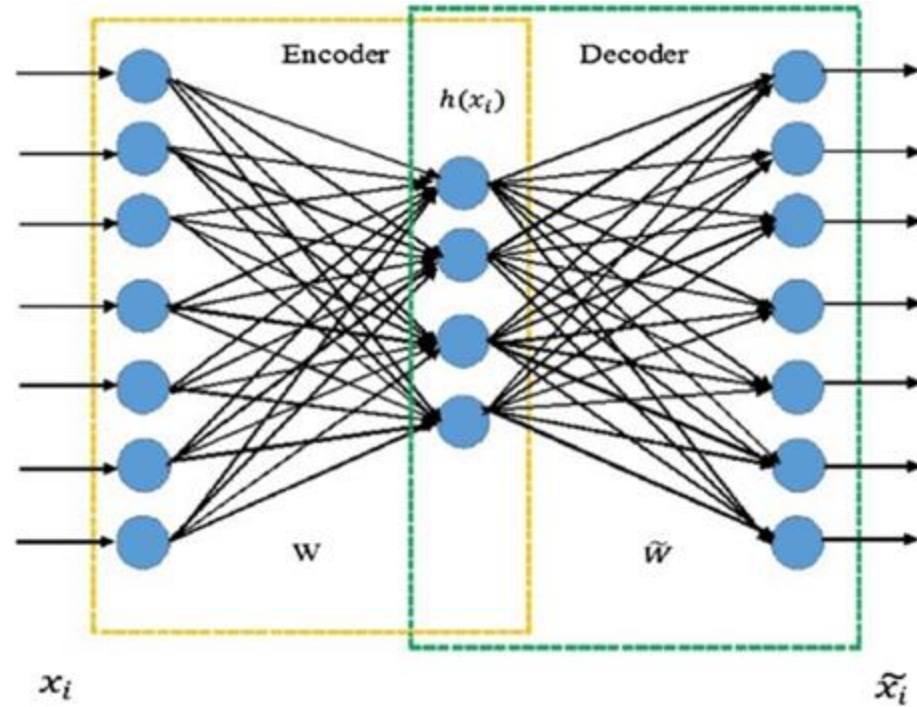
- Increasing popularity and higher accuracy in many applications;

Research Objectives:

Explore deep learning approach for unsupervised feature learning, such that:

- features are data-driven;
- features are noise-free;
- features are compact;
- features are extracted using full spectra bands;
- features are non-linear;
- using the features can improve LUT inversion approaches for better satisfying the operational requirements of incoming big hyperspectral data.

Autoencoder Architecture



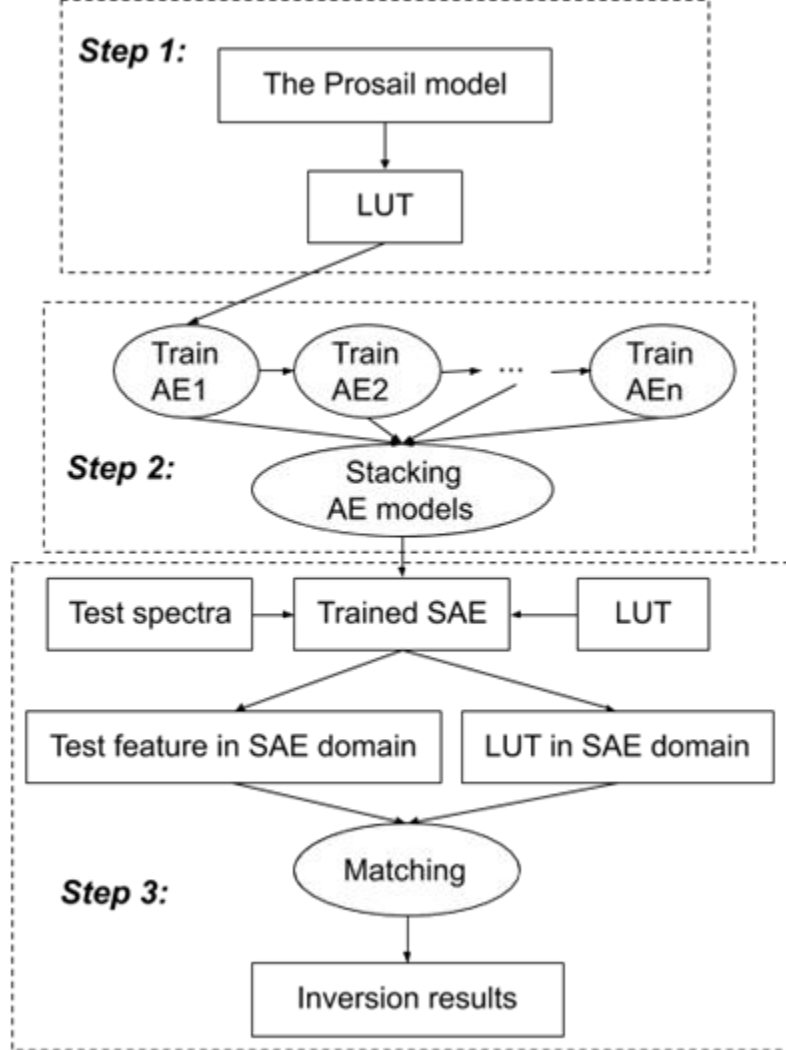
Stacked Autoencoder



Stacked AutoEncoder: Advantages

- **Unsupervised feature learning** approach which does not requires training data or prior knowledge of the problem;
- **Deep nonlinear feature** transformation for better capturing discriminative information in the spectral domain;
- Features are **compact and noise-free**;
- Fast due to **GPU** computation;

Overview of the Methodology

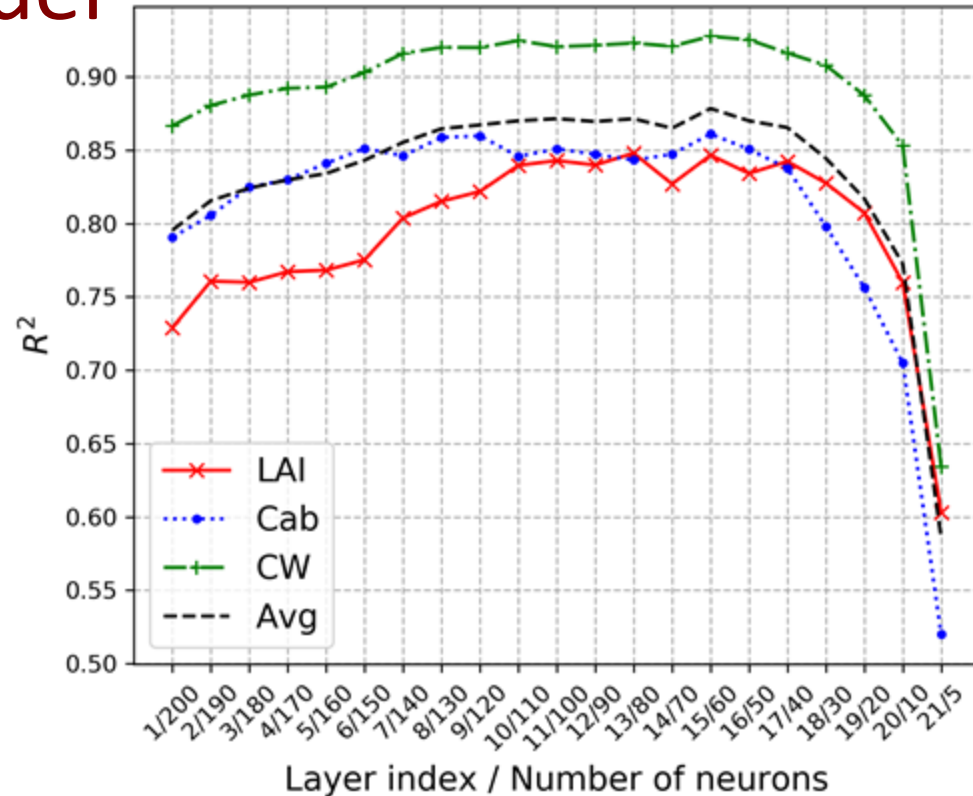


- **Step 1:** LUT generation;
- **Step 2:** Learning SAE features;
- **Step 3:** LUT inversion of Prosail in SAE feature domain;

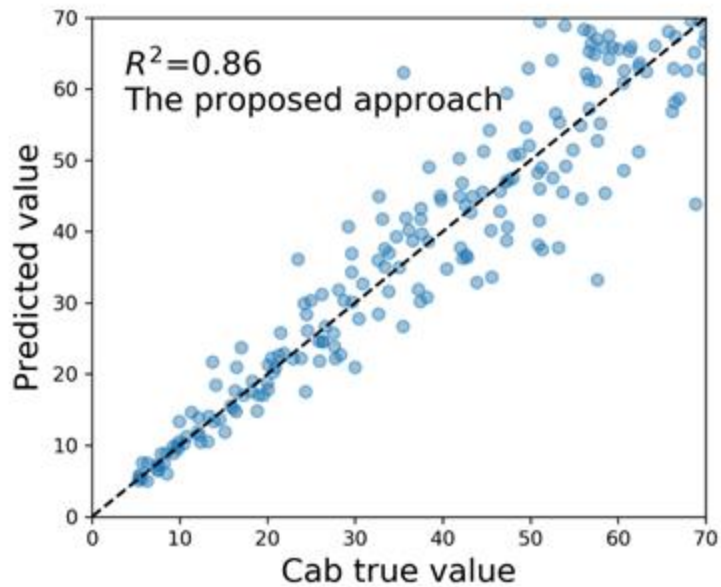
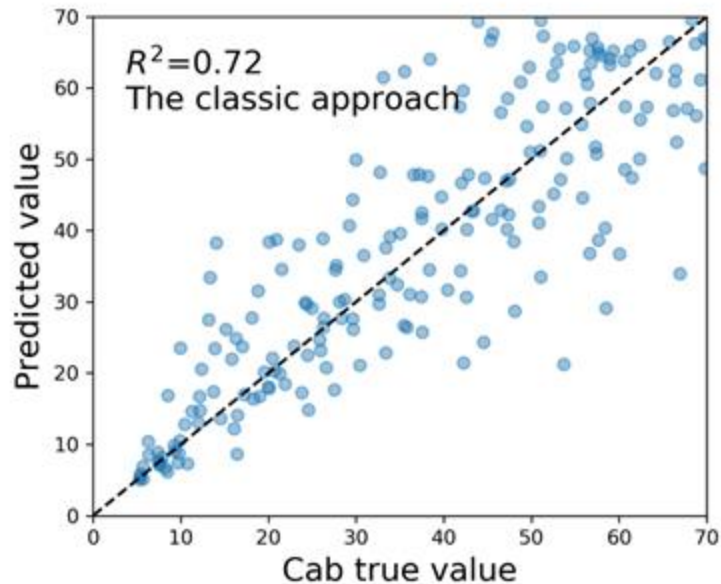
Simulated study

- Step 1: Simulate data using the Prosail model, and generate LUT
- Step 2: Training SAE for feature extraction;
- Step 3: Test LUT inversion using simulated test data;

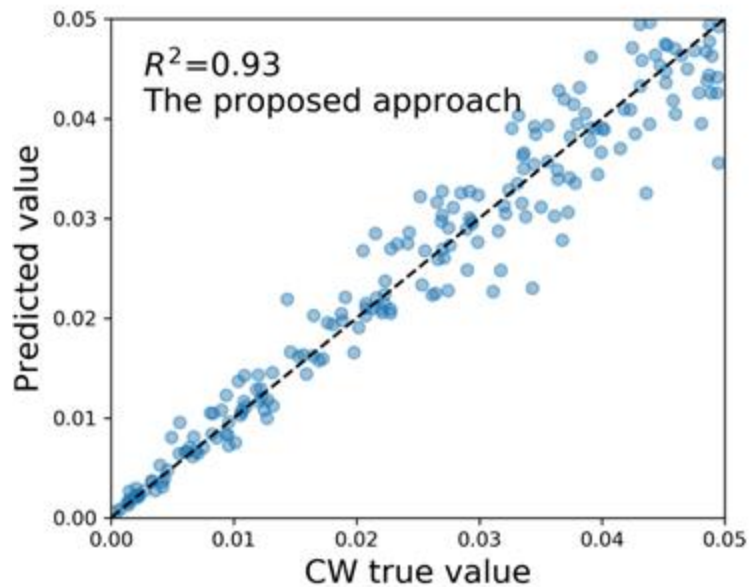
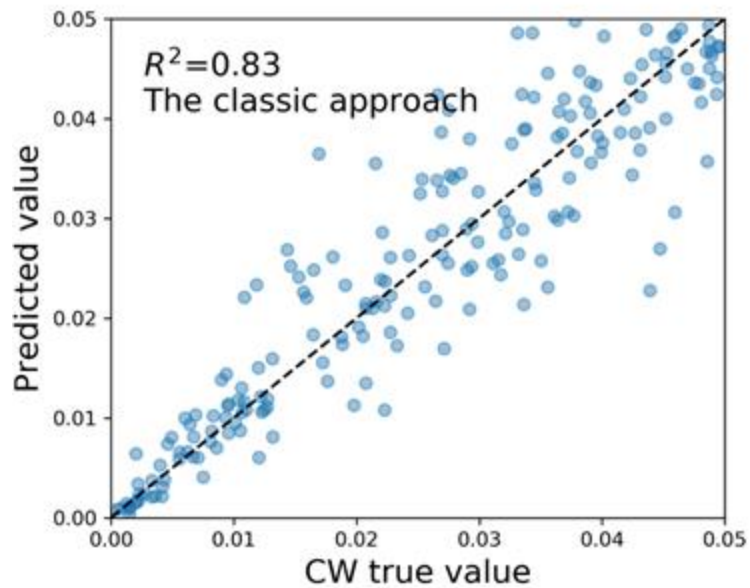
Performance variation with the “deepness” of the model



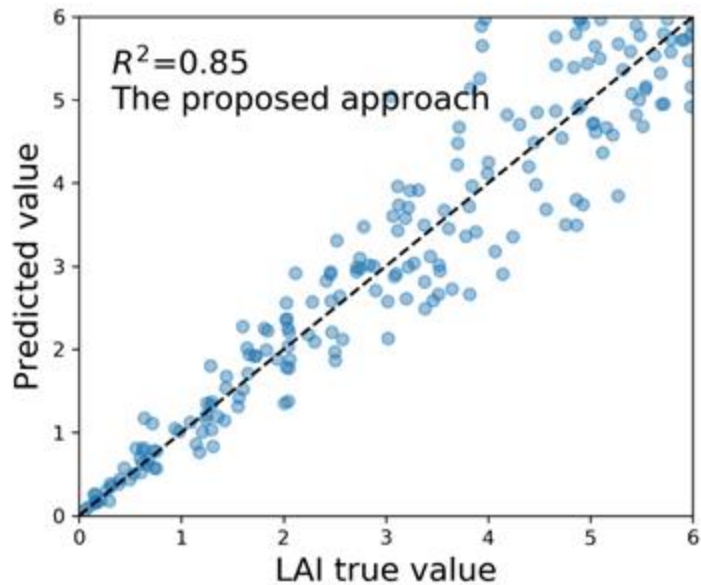
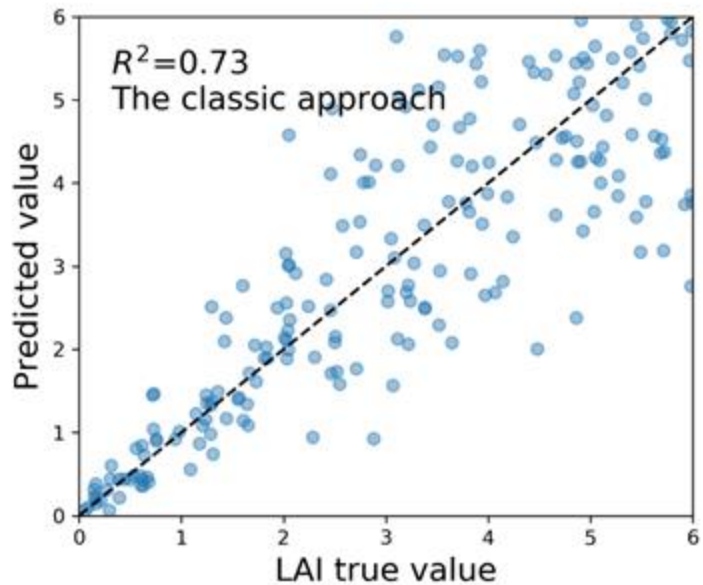
Results on Simulated Image using Prosail



Results on Simulated Image using Prosail



Results on Simulated Image using Prosail



Experiments on real UAV hyperspectral data

- Step 1: Simulate data using the Prosail model, and generate LUT
- Step 2: Training SAE for feature extraction;
- Step 3: Perform LUT inversion of real hyperspectral image collected in 2018 by the Headwall UAV hyperspectral system over a vineyard near Toronto;

PRODUCT DATA SHEET



Nano-Hyperspec®

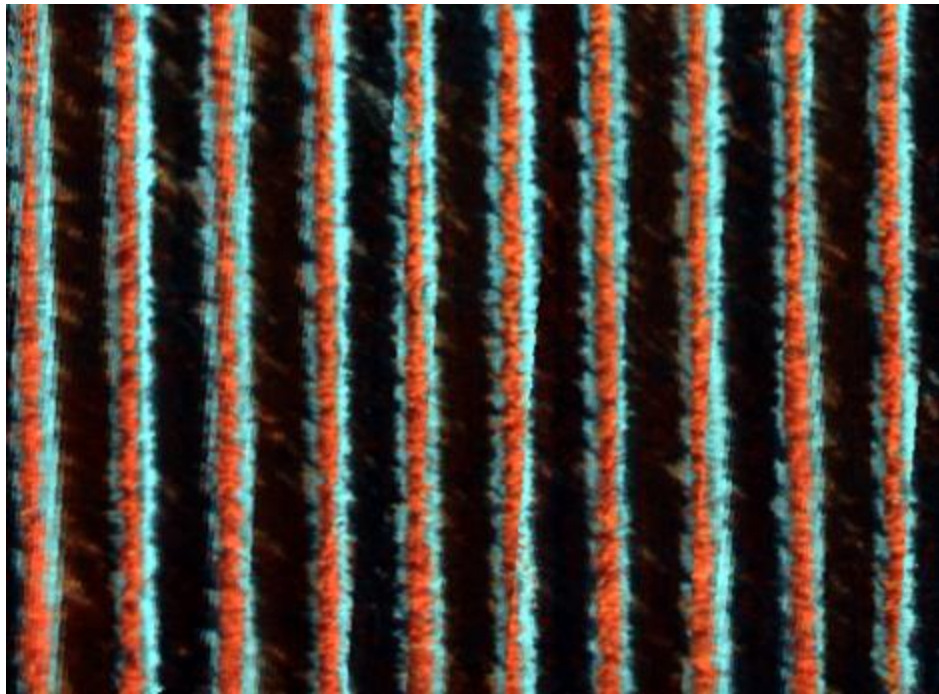
Wavelength range	400-1000 nm
Spatial bands	640
Spectral bands	270
Dispersion/Pixel (nm/pixel)	2.2
FWHM Slit Image	6 nm
Integrated 2 nd order filter	Yes
f/#	2.5
Layout	Aberration-corrected concentric
Entrance Slit width	20 μm
Camera technology	CMOS
Bit depth	12-bit
Max Frame Rate (Hz)	350
Detector pixel pitch	7.4 μm
Max Power (W)	13
Storage capacity	480GB (~130 minutes at 100 fps)
Weight without lens, GPS (lb / kg)	1.2 / 0.5
Operating Temperature	0° C to 50° C

PERFECT FOR UAV APPLICATIONS





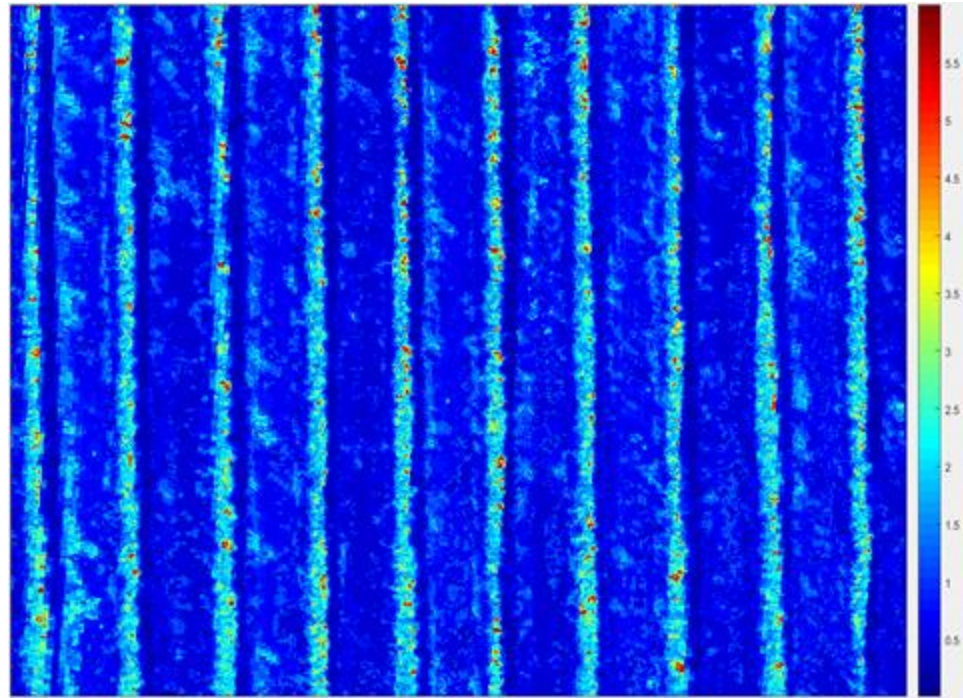
RGB Image



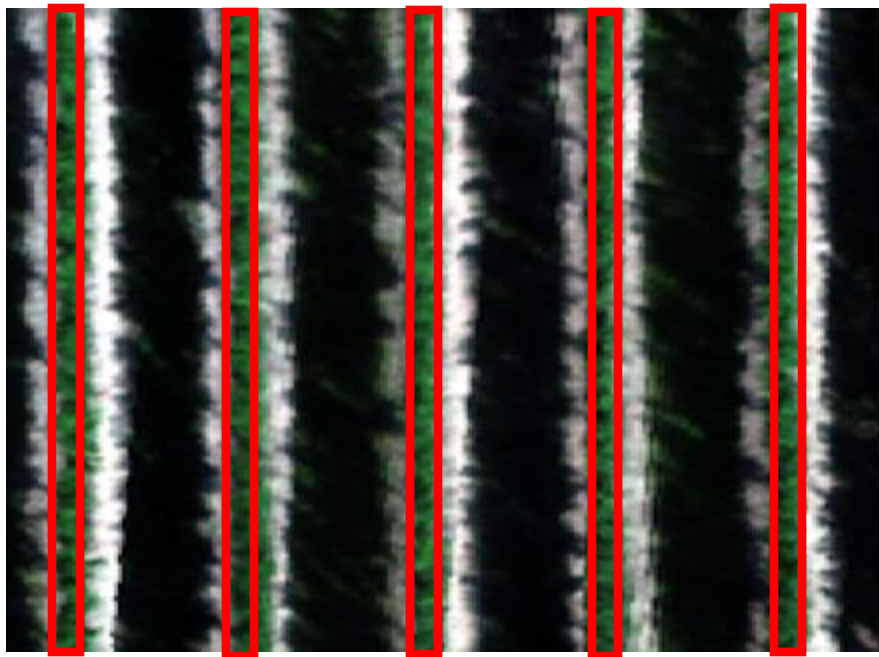
Pseudo RGB Image



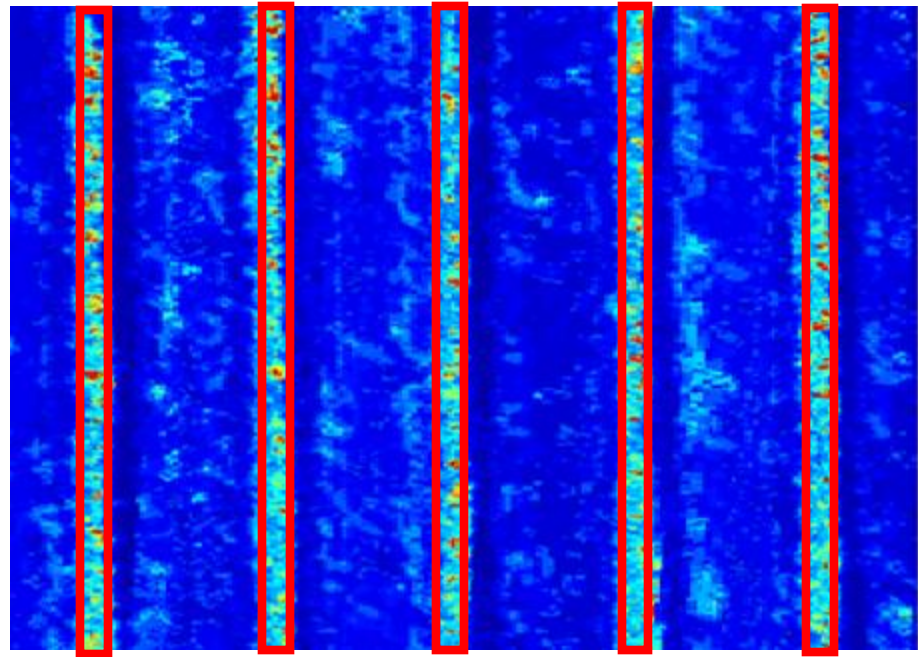
RGB Image



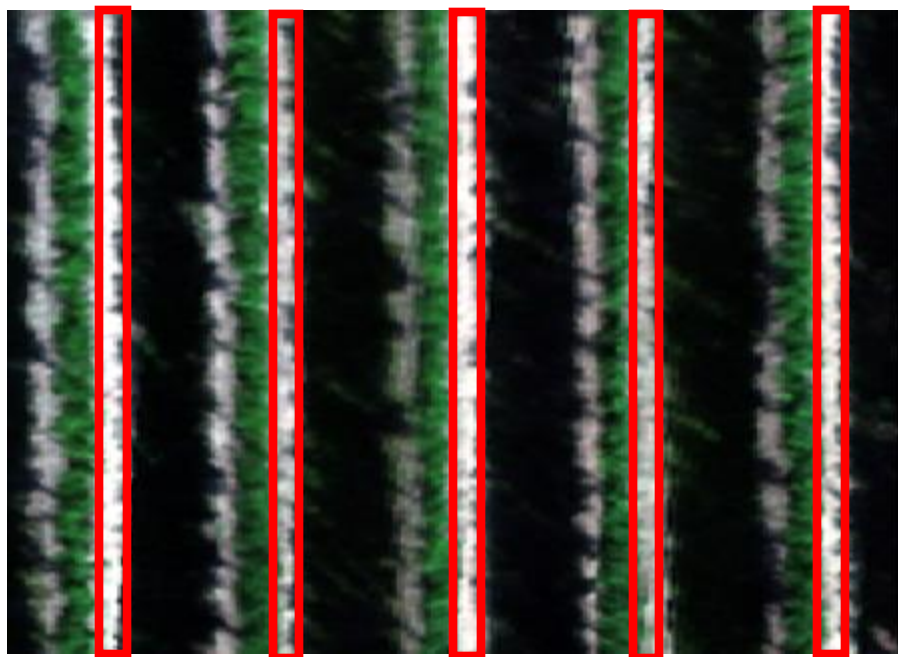
Estimated LAI



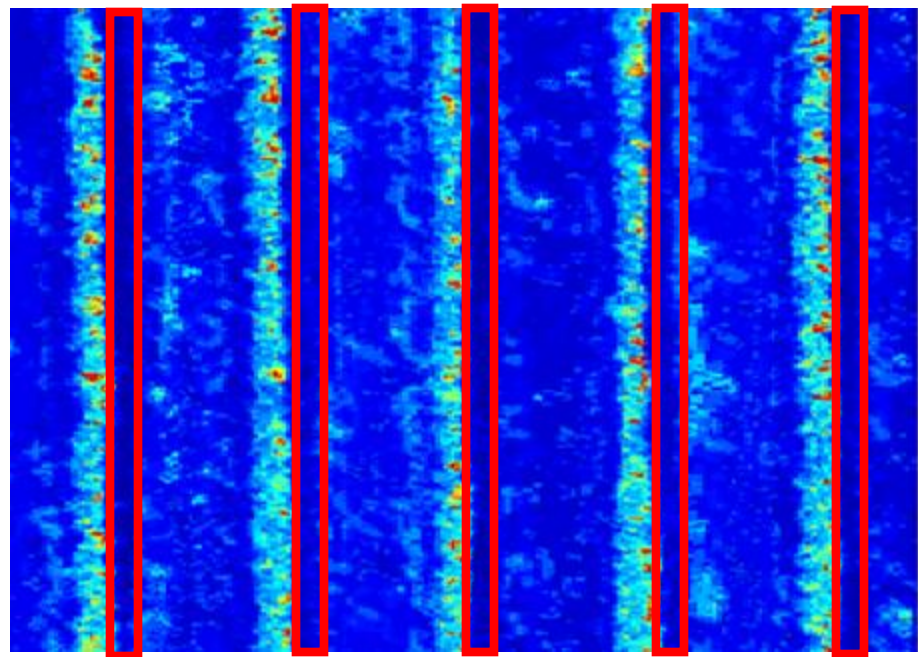
RGB Image



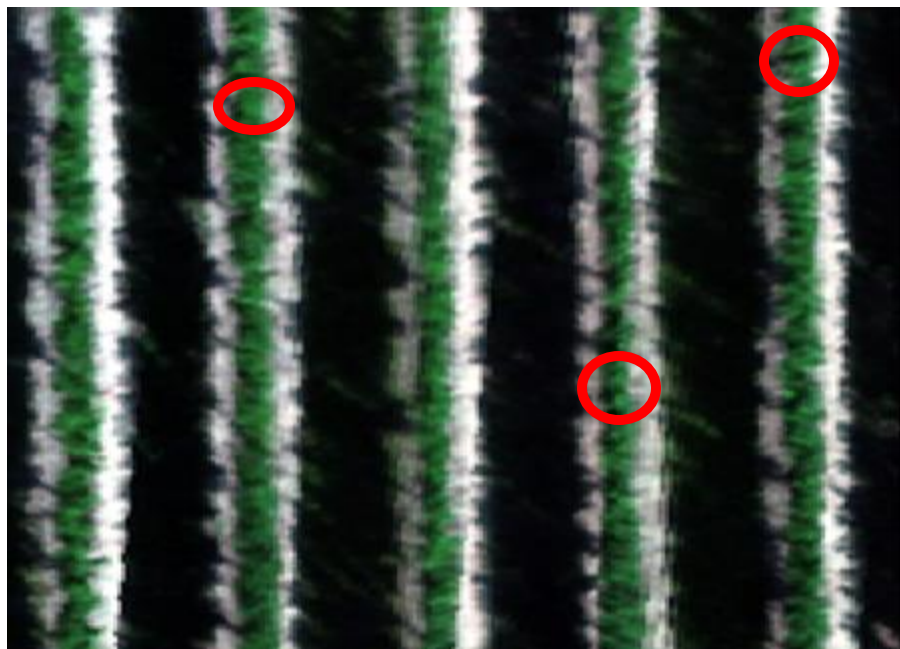
Estimated LAI



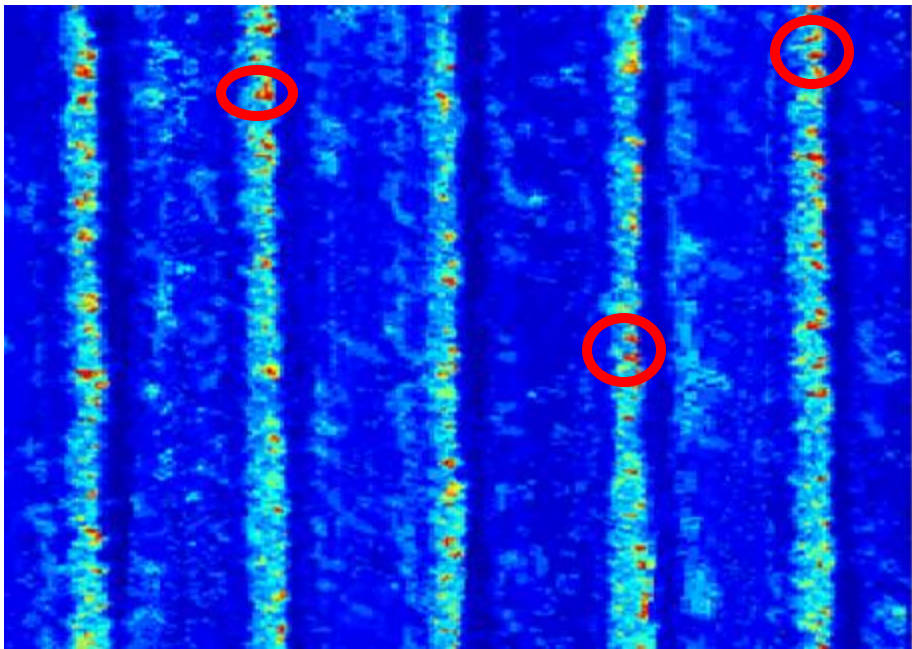
RGB Image



Estimated LAI



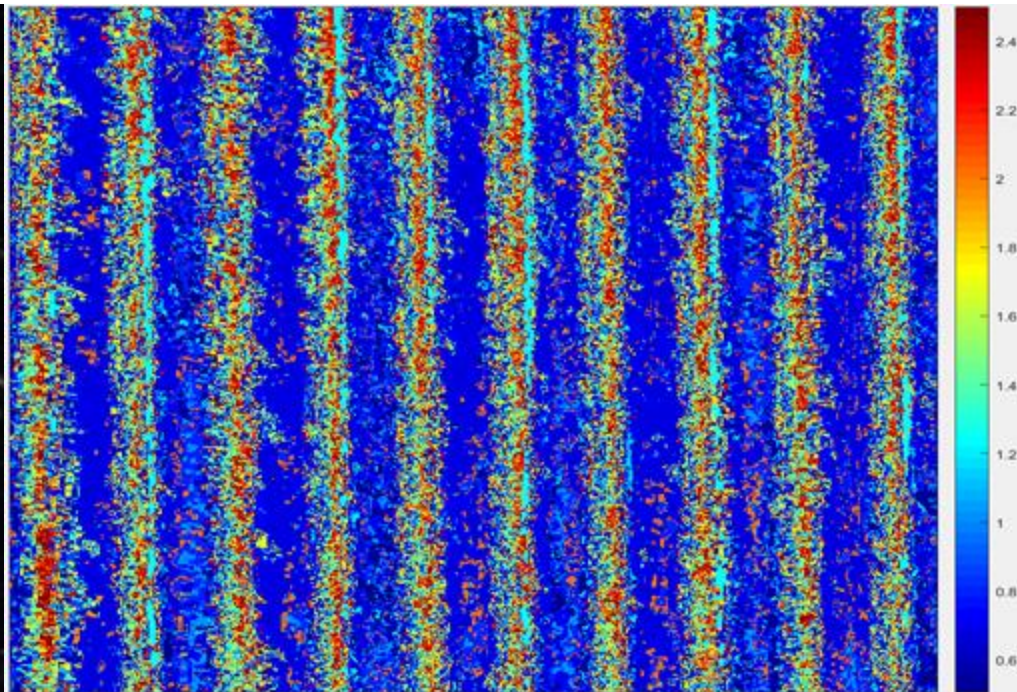
RGB Image



Estimated LAI



RGB Image



Estimated leaf
structure parameter

Processing time for a 512-by-512 image

Approaches	Time used for LUT inversion
272 channels under CPU	28.23 minutes
50 SAE features under GPU	2.01 seconds

Conclusions:

- The SAE features has potential to **improve both the accuracy and computation efficiency** of the LUT inversion of Prosail model;
- The proposed LUT inversion in SAE feature domain can better **handle the challenges of big hyperspectral data** in many vegetation monitoring applications;

Article

Retrieval of Seasonal Leaf Area Index from Simulated EnMAP Data through Optimized LUT-Based Inversion of the PROSAIL Model

Matthias Locherer *, Tobias Hank, Martin Danner and Wolfram Mauser

Department of Geography, Ludwig-Maximilians-Universität München, Luisenstraße 37, D-80333 Munich, Germany; E-Mails: tobias.hank@lmu.de (T.H.); martin.danner@iggf.geo.uni-muenchen.de (M.D.); w.mauser@lmu.de (W.M.)

* Author to whom correspondence should be addressed; E-Mail: m.locherer@iggf.geo.uni-muenchen.de; Tel.: +49-89-2180-6695; Fax: +49-89-2180-6675.

Academic Editors: Saskia Foerster, Véronique Carrere, Michael Rast, Karl Staenz and Prasad S. Thenkabail

Abstract: The upcoming satellite mission EnMAP offers the opportunity to retrieve information on the seasonal development of vegetation parameters on a regional scale based on hyperspectral data. This study aims to investigate whether an analysis method for the retrieval of leaf area index (LAI), developed and validated on the 4 m resolution scale of six airborne datasets covering the 2012 growing period, is transferable to the spaceborne 30 m resolution scale of the future EnMAP mission. The widely used PROSAIL model is applied to generate look-up-table (LUT) libraries, by which the model is inverted to derive LAI information. With the goal of defining the impact of different selection criteria in the inversion process, different techniques for the LUT based inversion are tested, such as several cost functions, type and amount of artificial noise, number of considered solutions and type of averaging method. The optimal inversion procedure (Laplace, median, 4% inverse multiplicative noise, 350 out of 100,000 averages) is identified by validating the results against corresponding *in-situ* measurements ($n = 330$) of LAI. Finally, the best performing LUT inversion ($R^2 = 0.65$, RMSE = 0.64) is adapted to simulated EnMAP data, generated from the airborne acquisitions. The comparison of the retrieval results to upscaled maps of LAI, previously validated on the 4 m scale, shows that the optimized retrieval method can successfully be transferred to spaceborne EnMAP data.

Data

1. Prosail simulation of AVIS-3

2. strategies. The airborne imaging spectrometer AVIS-3 (Airborne Visible and Near Infrared Spectrometer, LMU, Munich, Germany), developed at the Department of Geography of the Ludwig Maximilian University (LMU) [19], was used to perform four imaging flights during the course of the vegetation period of 2012 over a 12 km² large test site in Southern Germany (Neusling, Lower Bavaria, central coordinates: 48.69 N, 12.87 E). The seasonal campaign was complemented by two additional acquisitions from the airborne sensor HySpex, which is operated by the German Aerospace Center (DLR) [20].

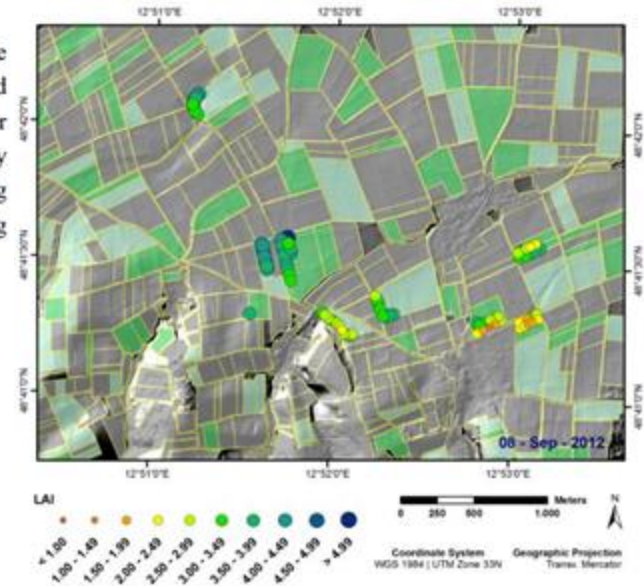
In order to validate the methods developed for the retrieval of biophysical parameters, an extensive field campaign was carried out alongside the airborne data acquisitions, resulting in more than 330 valid LAI measurements of five different crops. These represent the major crops cultivated in the area (winter wheat, winter barley, rapeseed, maize, sugar beet). The LAI measurements were conducted non-destructively using LAI-2000 plant canopy analyzers (Li-Cor, Lincoln, NE, USA), applying a diagonal sampling pattern (two reference and eight canopy measurements) within elementary sampling units corresponding to the geometric resolution of the airborne data.

1. Prosail simulation of Enmap

2. AVIS-3 simulation of Enmap

Table 1. Airborne data acquisitions over the Neusling test site.

Acquisition Date	Sensor	Sun Zenith (°)	Sun Azimuth (°)
28 April	AVIS-3	42	132
8 May	HySpex	45	115
25 May	AVIS-3	39	236
16 June	AVIS-3	28	146
12 August	HySpex	42	133
8 September	AVIS-3	45	155



Preprocessing of Airborne data - why additional channels?

The preprocessing of the airborne data, which also was carried out at LMU for the AVIS-flights, includes analysis of the spectral properties, sensor calibration, geometric correction, spatial data fusion, radiometric calibration and finally spectral data fusion. Using in-situ measurements conducted with a calibrated ASD FieldSpec 4, the raw data was finally calibrated to bottom of atmosphere (BOA) reflectance by empirical alignment. Having gone through all corrective steps, AVIS-3 data consists of 197 spectral bands, covering a spectral range from 477–1704 nm at a spectral resolution of 5.8 nm (<994 nm) and 6.6 nm (>994 nm), respectively. The ground sampling distance (GSD) in this case was 4 m. An important step of the preprocessing is the consideration of viewing angle information. **For this purpose, sensor zenith and azimuth angle were stacked to the spectral data as additional bands. If this meta information is available in conjunction with the respective solar zenith angle of the acquisition time, the illumination geometry can be traced for each pixel.**

The HySpex data was acquired and preprocessed by DLR, atmospherically corrected by the use of ATCOR [21], and provided as BOA reflectance with a GSD of 4 m, equal to the AVIS-3 data. The spectral properties of HySpex were adapted to those of AVIS-3, according to the spectral response functions of the latter, which is assumed to correspond to a Gaussian distribution around the center wavelength of each band. This results in a full width half maximum (FWHM) equal to the sampling interval of the sensor. Further, sensor zenith and azimuth information was added as separate bands to the HySpex data in order to conform to the specifications of the processed AVIS-3 data.

AVIS-3 simulation of EnMap data - why radiance to DN value?

To examine the applicability of the methods investigated in this study to the upcoming EnMAP-Hyper Spectral Imager (HSI), the airborne hyperspectral datasets of the study site had to be modified to meet the spatial, spectral and radiometric properties of the future satellite sensor. For that

purpose, Segl *et al.* [22] have developed the EnMAP End-to-End Simulator (EeteS), by which the image data from the multiseasonal campaign was converted into simulated EnMAP data. During forward simulation, EeteS uses several modules for the simulation of atmospheric effects and sensor properties (radiometric, spectral and spatial) and converts the airborne reflectance to realistic raw top of atmosphere (TOA) data. It is coupled with the backward simulation tool encompassing on-board L1-calibration of non-linearity and dark current correction as well as absolute radiometric calibration. The radiometric module converts the data from at-sensor radiance to digital numbers by taking into account a range of influence parameters, such as integration time, quantum efficiency (QE), different kinds of noise, infrared background signal, high/low gain modes for the VNIR detector, variable offsets and gains, as well as an individual non-linear response for each detector element. This is an important step, because these parameters define the sensor-dependent noise, as specified by the detector manufacturer. The subsequent L2-processors of co-registration, atmospheric correction and ortho-rectification complete the tool. This allows the generation of artificial satellite data, which incorporates the instrumental and environmental configurations of the future EnMAP-HSI.

It should be noted that the EnMAP simulations used in this study are restricted to spectral information within the spectral range of AVIS-3, *i.e.*, from 471–1753 nm. Although the simulation includes the full EnMAP spectral range (420–2450 nm), all bands in the simulated data below 471 and beyond 1753 nm contain no information.

Prosail simulation of AVIS-3 - Influence of discretion level?

The quality of a LUT depends on the range, discretion levels, number of parameter configurations as well as on an optimal search strategy [24]. If the distance between the discretion levels is too far or the dimension is too low, the LUT inversion may lead to suboptimal solutions [23]. Similar to neural networks, which have to be trained before parameter retrieval, an advantage of the LUT is that a large amount of the computing time is completed before the actual application. This antecedent calculation is based on various input parameters [24]. In contrast to numerical optimization and also to ANNs, the LUT approach admits a global search and is in this way not in danger of being trapped in local minima [25].

Numerous studies, e.g., [26,27], showed that the LUTs are often more robust and generate higher accuracies compared to other RTM inversion approaches. Moreover, LUTs have the advantage that they represent a relatively simple method, their content being precisely defined. In this way, intermediate results can also be considered as comprehensive, while neural networks are often criticized as being black boxes [24]. In order to overcome these drawbacks, recently also machine learning algorithms that follow a gray box behavior and thus provide more transparency are emerging [28]. Compared to iterative optimization algorithms, the LUT method is significantly less time consuming [29]. However, it is not as fast as a neural network. Due to its advantages, the LUT approach was chosen to serve as the inversion technique for

Prosail simulation of AVIS-3 - Influence of LUT size, why Gaussian?

reflectance values stored in column direction, **the LUT also includes the corresponding input parameters by which the modeled reflectance spectrum was generated.**

Subsequently, the size of the LUT in row direction was specified, defining the number of reflectance spectra available for the comparative analysis with measured reflectance signals. If the size is too small, the estimation accuracy may suffer. By contrast, a too large number of modeled spectra would lead to an increase in computation time, without adding value in terms of accuracy after a certain accuracy level has been reached. Weiss *et al.* [30] investigated the effect of the LUT size on the accuracy of canopy variables. They tested several LUTs ranging from 25,000–280,000 in row size and found that an LUT based on 100,000 modeled spectra provides an optimal compromise between model accuracy and required computer-resources. Based on this finding, we randomly combined the input parameters to the model in 100,000 instances, each following a distribution within a specific range. Instead of using a uniform distribution, the input parameters were defined to follow a Gaussian distribution according to their most probable incidence during a growing season in Southern Germany. This procedure has the advantage that the most likely variable values can be distinguished in finer steps, which increases model accuracy. However, the accuracy for less likely variable values may suffer from less frequent cases. The Gaussian distribution was chosen over other distribution functions, since the aim of this study is to estimate parameters within a growing period. It is thus not expected that the variables under examination, e.g., LAI, show very rapid increases, or even extreme values, but rather that they develop gradually. Table 2 shows the range and distribution of each PROSAIL input parameter as defined in this study. The individual settings are based on experiences and empirical values from several studies [31–33]. These values only were slightly modified to guarantee that the expected variability of the target variables expected during one growing season was covered. The selection of the parameters stored in the LUT therefore was independent from *in-situ* observations. It should be noted that due to its negligible effect, the ratio of diffuse to total incident radiation was constantly set to 10%.

Table 2. Distribution of PROSAIL input parameters for the generation of the LUT.

Model	Parameter	Min	Max	Mean	Std. Dev.
PROSPECT-5b	Leaf chlorophyll content [$\mu\text{g}/\text{cm}^2$]	0	90	50	40
	Leaf carotenoid content [$\mu\text{g}/\text{cm}^2$]	0	20	10	7
	Brown pigment content [-]	0	1.5	0.2	0.8
	Equivalent water thickness [cm]	0	0.05	0.02	0.025
	Leaf mass per unit leaf area [g/cm^2]	0	0.02	0.01	0.01
	Structure coefficient [-]	1	2.5	1.5	1
4SAIL	Average leaf angle [$^\circ$]	30	80	60	20
	Leaf area index [m^2/m^2]	0	7	3.5	2.5
	Hot spot [-]	0	1	0.45	0.6
	Soil coefficient [-]	0	1	0.5	0.5

Prosail simulation of AVIS-3 - How to account for Geometry Influence?

During this step, parameters describing the illumination geometry, *i.e.*, solar zenith angle, observer zenith and azimuth angle, were fixed and are therefore identical in each of the 100,000 combinations. Nevertheless, due to varying viewing angles in the 2012 images, the anticipated BRDF effects must be taken into account. This is necessary because different angle settings affect reflectance in a non-negligible fashion. To solve this problem, the LUT was generated repeatedly for several categories of observer zenith and azimuth angles. The step size of zenith angles was set to 5 °, covering a range from -25 ° to +25 °. The required range was determined by the highest and lowest observer zenith angles

in all available images of the 2012 campaign. For the relative azimuth angle, a step size of 10 ° in a range from 0 °-180 ° was chosen in order to cover all potential observer angles occurring in the image data. In order to take the solar zenith angles of the six different flights into account, the steps of calculating the LUT for each possible observer angle class combination were repeated once more, this time considering the respective solar zenith angle of each of the six flights. However, four iterations were sufficient, because for the first and fifth as well as for the second and sixth flights the solar zenith angles were almost identical (Table 1). It must be noted that topographic effects on illumination geometry could be neglected due to the flat surface of the test area. As a consequence, the dimension of the generated LUT library is defined by the product of the biophysical input parameters ($n = 100,000$), the observer zenith angle classes ($n = 11$), the observer azimuth classes ($n = 19$) and the solar zenith angle classes ($n = 4$), resulting in a total of 83,600,000 reflectance spectra including their corresponding parameter specifications being stored in the LUT.

Table 1. Airborne data acquisitions over the Neusling test site.

Acquisition Date	Sensor	Sun Zenith (°)	Sun Azimuth (°)
28 April	AVIS-3	42	132
8 May	HySpex	45	115
25 May	AVIS-3	39	236
16 June	AVIS-3	28	146
12 August	HySpex	42	133
8 September	AVIS-3	45	155

Prosail simulation of AVIS-3 - How to account for Geometry Influence?

When applying the inversion sequence to an image, the algorithm starts with the identification of the respective solar zenith angle. The program identifies the first pixel and extracts the observer angle information, which is stored in the additional bands 198 (zenith) and 199 (azimuth) of the AVIS-3/HySpex data. The relative azimuth is calculated based on the latter and on the manually supplied solar azimuth angle. According to the now specified angle information, the corresponding table, equaling the size of the initial LUT of 100,000 spectra, is loaded from the LUT library. Based on a cost function, a curve fitting is subsequently performed, whereby best match(es) between the measured spectrum and the modeled spectra are identified. When completed, the algorithm collects the corresponding metadata of the best fit(s) and stores it with the equivalent pixel of the output image. The success of the parameter retrieval thereby depends on certain important selection criteria at various steps within the inversion sequence. The most critical are the precise choice of the data ranges that are compared, the cost function applied in the curve fitting process, and the management of the result of the curve fitting. These criteria are individually investigated in the following.

Table 1. Airborne data acquisitions over the Neusling test site.

Acquisition Date	Sensor	Sun Zenith (°)	Sun Azimuth (°)
28 April	AVIS-3	42	132
8 May	HySpex	45	115
25 May	AVIS-3	39	236
16 June	AVIS-3	28	146
12 August	HySpex	42	133
8 September	AVIS-3	45	155

Prosail simulation AVIS-3 - Why band selection

The first criterion is the selection of bands to be used for the comparison of the measured and simulated reflectance. Since the quality of reflectance data might differ among the available bands mostly due to noise, they must be selected wisely to avoid potentially corrupt results. **Many studies (e.g., [34,35]) found that an appropriate band selection, or, alternatively, a specific weighting of different spectral bands, leads to an improvement in the inversion quality and prevents biases in the parameter estimation. Making an informed selection is, however, not trivial.** A strategy to consider is the one proposed by Darvishzadeh *et al.* [25], who suggested discarding those wavelengths that are not well simulated by PROSAIL using an iterative approach, starting with the elimination of the worst modeled spectral band among all sample plots. The LUT inversion is repeated until all bands show acceptable accuracies within a user-specified threshold.

In view of the expected spectral capacity of EnMAP, which will provide spectrally contiguous data, a different approach was applied in this study by neglecting band selection apart from atmospherically distorted bands. This was based on the assumption that an applied curve fitting would be the more precise the more bands are considered and is related to the fact that the contiguous spectrum contains more information, e.g., on specific absorption ranges, than a multispectral dataset. Although the use of all available bands may provide redundant information when trying to retrieve individual parameters, e.g., LAI, this method has the advantage that some surface parameters, affecting reflectance in different and in some cases very small wavelength ranges, can be derived by a uniform method. Consequently, after excluding the bands located within the atmospheric water vapor absorption range and some bands with reduced sensitivity, located at the marginal areas of the CCDs, the remaining 146 bands were finally used in the inversion process.

Prosail simulation AVIS-3 - Why adding noise

A fundamental difference between simulated and measured reflectance, which was gathered by the use of airborne sensors, is the fact that the latter is affected by uncertainties originating from measurement inaccuracies and from the preprocessing steps of sensor calibration, geometric correction and radiometric calibration. On the other hand, the reflectance model might produce uncertainties as well, which are associated with its complex architecture for the calculation of canopy radiative transfer [33].

Compensating the uncertainties of both, sensor data and potential model weaknesses, is the reason for adding noise to the data. The type and amount of noise introduced differs in studies found in the literature. Bacour *et al.* [31], e.g., added 4% white Gaussian noise with no bias to the data. Baret *et al.* [32], by contrast, added white Gaussian noise to the reflectance values, which has an absolute value of 0.04. A combination of both with an additive level of 0.01 and a multiplicative level of 4% was used by Verger *et al.* [33]. In a study by Verrelst *et al.* [36], a systematic approach was pursued, which examined the effect of adding 0%–30% Gaussian noise to the data in 1% intervals. A modified approach was investigated by Rivera *et al.* [37] in which the influence of a multiplicative noise ranging from 0%–50%, in 2% intervals, was tested.

Prosail simulation AVIS-3 - Why different noises

Comparable to the latter two studies, an approach combining different noise types was adopted to identify the noise level leading to the best possible results in this study. In this approach, both additive and multiplicative Gaussian noise as well as a combination of both was used. Of decisive importance for the amount of noise is the variance (σ^2) in the Gaussian distribution [36].

Since the impact of multiplicative noise on the reflectance depends on the individual value of each band, high reflectance values, for example those occurring in the red edge, obtain higher noise values than low reflectances. However, low reflectance values are typically more prone to noise due to a lower light intensity reaching the sensor, which results in a lower signal-to-noise ratio (SNR) for band. Therefore, an inverse form of multiplicative noise, having a stronger impact on low values than on high values, was tested as well. This is achieved by simply subtracting the reflectance value at the given wavelengths, which can range from 0–1, from the high reflectance value of 1. A total of five types of noise were defined for this study and tested their performance. They are described by Equations (1)–(5):

Additive noise (Equation (1))

$$R_{ns}(\lambda) = R_{sim}(\lambda) + \chi(0, \sigma(\lambda)) \quad (1)$$

Multiplicative noise (Equation (2))

$$R_{ns}(\lambda) = R_{sim}(\lambda) \times [1 + \chi(0, \sigma(\lambda))] \quad (2)$$

Inverse-multiplicative noise (Equation (3))

$$R_{ns}(\lambda) = 1 - \{[1 - R_{sim}(\lambda)] \times [1 + \chi(0, \sigma(\lambda))]\} \quad (3)$$

Combined noise (Equation (4))

$$R_{ns}(\lambda) = R_{sim}(\lambda) \times [1 + \chi(0, 2\sigma(\lambda))] + \chi(0, \sigma(\lambda)) \quad (4)$$

Inverse-combined noise (Equation (5))

$$R_{ns}(\lambda) = 1 - \{[1 - R_{sim}(\lambda)] \times [1 + \chi(0, 2\sigma(\lambda))]\} + \chi(0, \sigma(\lambda)) \quad (5)$$

where

$R_{ns}(\lambda)$	simulated reflectance value for band λ with noise
$R_{sim}(\lambda)$	simulated reflectance value for band λ
$\chi(0, \sigma)$	Gaussian distribution (mean value 0 and standard deviation σ)
$\sigma(\lambda)$	uncertainties within the Gaussian distribution for band λ

In order to account for the fact that a given variance value has a less pronounced effect when applied as multiplicative noise, it is double-weighted compared to the additive noise factor in the combined methods.

Prosail simulation AVIS-3 - Cost function - Why LP is more robust?

The cost function measures the discrepancies between observed and simulated reflectance values [13] and therefore serves for the purpose of identifying the combination by which the error between the simulated data provided by the LUT and the measured reflectance is minimized. Recently, several studies have investigated the potential of alternative cost functions for the retrieval of best fits between measured and simulated data (e.g., [36–38]). One of the most common measures in this context is the root mean square

error (RMSE), which has been applied in several studies (e.g., [23,26,31]). For this reason, it was chosen as one of the cost functions applied in this study. The widely used least-square estimators (L2-means) produce good results, when the underlying assumptions, such as noise is Gaussian, are true [37]. Two further L2-estimators, *i.e.*, Nash-Sutcliffe Efficiency (NSE) [39] and Geman & McClure Estimator (GM) [40], and a L1-estimator (absolute value), which is represented by the Laplace Distribution (LP) [40], were tested. The NSE is a measure of the mean square error to the observed variance, and is sensitive to large errors [39]. Among all cost functions, the very general Laplace Distribution represents the simplest one. This L1-estimator calculates the distance, or, in other words, the area, between two spectra. As a result of its design, outlier values, which in general produce the largest errors, exert a less pronounced influence on the overall result when compared to the NSE. This advantage is also the case for the GM. However, this last measure cannot guarantee the identification of a unique best fit [37], which is a general requirement of a robust M-estimator. The cost functions are described by Equations (6)–(9). It is noted that in this study, both the RMSE and the NSE are not only used as a cost function, they also support model validation.

$$RMSE = \sqrt{\frac{1}{n} \sum_{\lambda=1}^n (R_{msd}(\lambda) - R_{sim}(\lambda))^2} \quad (6)$$

$$NSE = 1 - \frac{\sum_{\lambda=1}^n (R_{msd}(\lambda) - R_{sim}(\lambda))^2}{\sum_{\lambda=1}^n (R_{msd}(\lambda) - \bar{R}_{msd})^2} \quad (7)$$

$$GM = \sum_{\lambda=1}^n \frac{(R_{msd}(\lambda) - R_{sim}(\lambda))^2}{(1 + (R_{msd}(\lambda) - R_{sim}(\lambda))^2)} \quad (8)$$

$$LP = \sum_{\lambda=1}^n |R_{msd}(\lambda) - R_{sim}(\lambda)| \quad (9)$$

where

$R_{msd}(\lambda)$	measured reflectance at band λ
$R_{sim}(\lambda)$	simulated reflectance at band λ
\bar{R}_{msd}	mean of measured reflectance among all bands

Prosail simulation AVIS-3 - Cost function - Why LP is more robust?

The cost function measures the discrepancies between observed and simulated reflectance values [13] and therefore serves for the purpose of identifying the combination by which the error between the simulated data provided by the LUT and the measured reflectance is minimized. Recently, several studies have investigated the potential of alternative cost functions for the retrieval of best fits between measured and simulated data (e.g., [36–38]). One of the most common measures in this context is the root mean square

error (RMSE), which has been applied in several studies (e.g., [23,26,31]). For this reason, it was chosen as one of the cost functions applied in this study. The widely used least-square estimators (L2-means) produce good results, when the underlying assumptions, such as noise is Gaussian, are true [37]. Two further L2-estimators, *i.e.*, Nash-Sutcliffe Efficiency (NSE) [39] and Geman & McClure Estimator (GM) [40], and a L1-estimator (absolute value), which is represented by the Laplace Distribution (LP) [40], were tested. The NSE is a measure of the mean square error to the observed variance, and is sensitive to large errors [39]. Among all cost functions, the very general Laplace Distribution represents the simplest one. This L1-estimator calculates the distance, or, in other words, the area, between two spectra. As a result of its design, outlier values, which in general produce the largest errors, exert a less pronounced influence on the overall result when compared to the NSE. This advantage is also the case for the GM. However, this last measure cannot guarantee the identification of a unique best fit [37], which is a general requirement of a robust M-estimator. The cost functions are described by Equations (6)–(9). It is noted that in this study, both the RMSE and the NSE are not only used as a cost function, they also support model validation.

$$RMSE = \sqrt{\frac{1}{n} \sum_{\lambda=1}^n (R_{msd}(\lambda) - R_{sim}(\lambda))^2} \quad (6)$$

$$NSE = 1 - \frac{\sum_{\lambda=1}^n (R_{msd}(\lambda) - R_{sim}(\lambda))^2}{\sum_{\lambda=1}^n (R_{msd}(\lambda) - \bar{R}_{msd})^2} \quad (7)$$

$$GM = \sum_{\lambda=1}^n \frac{(R_{msd}(\lambda) - R_{sim}(\lambda))^2}{(1 + (R_{msd}(\lambda) - R_{sim}(\lambda))^2)} \quad (8)$$

$$LP = \sum_{\lambda=1}^n |R_{msd}(\lambda) - R_{sim}(\lambda)| \quad (9)$$

where

$R_{msd}(\lambda)$	measured reflectance at band λ
$R_{sim}(\lambda)$	simulated reflectance at band λ
\bar{R}_{msd}	mean of measured reflectance among all bands

Prosail inversion of AVIS-3 - why 17,640 inversions?

The *in-situ* measurements of LAI served as reference, enabling validation by comparing the field measurements to the retrieved information of the corresponding pixels. In order to incorporate as many of the above listed selection criteria as possible, an inversion loop was implemented, which is described in the following.

To find the optimized amount of noise for each type, the variance of the Gaussian distribution describing the noise was set to 21 different levels, beginning with 0%, which means that no noise was added, up to a maximum of 5%, 10% or 20%, depending on the noise type. Various ranges were chosen to take the different weighting that variance has for each noise type into account. In the next step, all four cost functions (Equations (6)–(9)) were used to search for the best fit between the measured and the (noisy) simulated data. To find the best strategy for mitigating the ill-posed problem, a total of 21 steps considering a predetermined number of solutions incorporating multiple solutions (best fits) were defined and averaged. The first step represents only the overall best fit, the second solution represents the average of the best 50 fits. The incorporation of additional fits is continued with step sizes of 50 additional spectra per solution until the last step, the 21st, is reached, which then takes 1000 spectra, *i.e.*, 1% of the complete LUT, into account. When averaged, both mean and median were used.

Since every possible combination of criteria within the defined range was calculated, the total number of single inversions is the product of different noise types ($n = 5$), various amounts of noise ($n = 21$), different cost functions ($n = 4$), number of best fits ($n = 21$) and the two separate averaging methods ($n = 2$). Consequently, a total of 17,640 singular inversions were conducted and each validated against the *in-situ* database of LAI.

Prosail inversion of AVIS-3 - which noise type best?

The comparison of the influence of the different noise types revealed that there is no significant difference in the model accuracies. The best results were obtained by inverse-multiplicative noise (NSE = 0.67), followed by additive and inverse-combined noise (NSE = 0.66). Despite the fact that the classical multiplicative noise performs worst (NSE = 0.65), implying that the assumptions that led to the implementation of an inverse mode of this noise type were correct, the differences in the highest accuracy achieved by the different modes are too small to be of meaningful relevance.

Additive noise (Equation (1))

$$R_{ns}(\lambda) = R_{sim}(\lambda) + \chi(0, \sigma(\lambda)) \quad (1)$$

Multiplicative noise (Equation (2))

$$R_{ns}(\lambda) = R_{sim}(\lambda) \times [1 + \chi(0, \sigma(\lambda))] \quad (2)$$

Inverse-multiplicative noise (Equation (3))

$$R_{ns}(\lambda) = 1 - \{[1 - R_{sim}(\lambda)] \times [1 + \chi(0, \sigma(\lambda))]\} \quad (3)$$

Combined noise (Equation (4))

$$R_{ns}(\lambda) = R_{sim}(\lambda) \times [1 + \chi(0, 2\sigma(\lambda))] + \chi(0, \sigma(\lambda)) \quad (4)$$

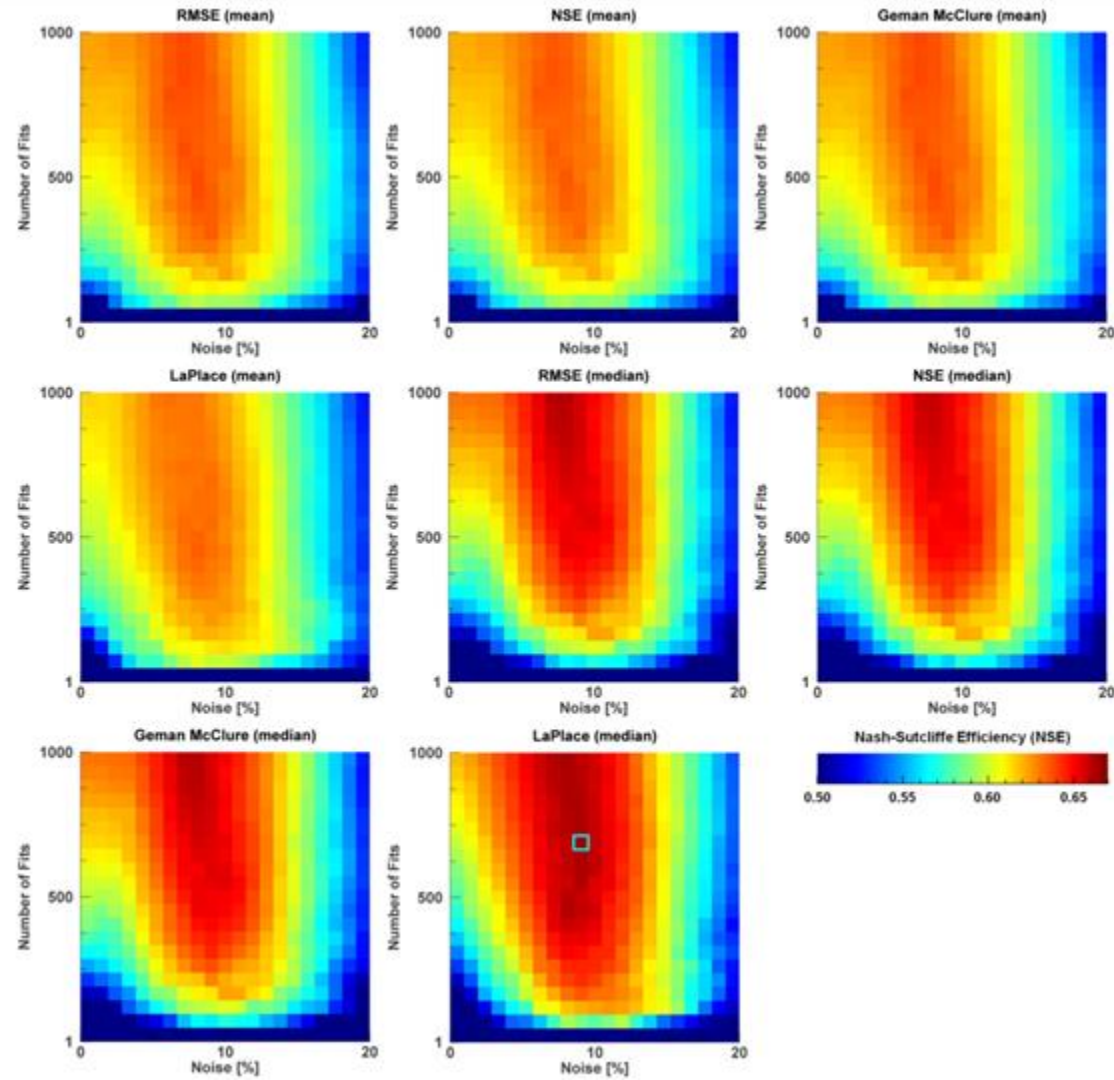
Inverse-combined noise (Equation (5))

$$R_{ns}(\lambda) = 1 - \{[1 - R_{sim}(\lambda)] \times [1 + \chi(0, 2\sigma(\lambda))]\} + \chi(0, \sigma(\lambda)) \quad (5)$$

where

$R_{ns}(\lambda)$	simulated reflectance value for band λ with noise
$R_{sim}(\lambda)$	simulated reflectance value for band λ
$\chi(0, \sigma)$	Gaussian distribution (mean value 0 and standard deviation σ)
$\sigma(\lambda)$	uncertainties within the Gaussian distribution for band λ

In order to account for the fact that a given variance value has a less pronounced effect when applied as multiplicative noise, it is double-weighted compared to the additive noise factor in the combined methods.



Prosail inversion of AVIS-3 results:

- (1) Median better than Mean, because of multiplicative noise?
- (2) Accuracy is low if noise level too high, or number of fits too low.
- (3) LaPlace better than other cost functions, because it is L1 and as such more robust to non-Gaussian noise?
- (4) Medium noise level leads to the best accuracy.

Based on the estimated vegetation parameters, the progressing development of specific crops throughout the growing season could be analyzed. Figure 6 shows the development of LAI for the investigated crops from 28 April to 8 September. The information was extracted from the retrieved parameter products by randomly choosing and averaging 30 pixels per scene and each crop type from the corresponding parameter.

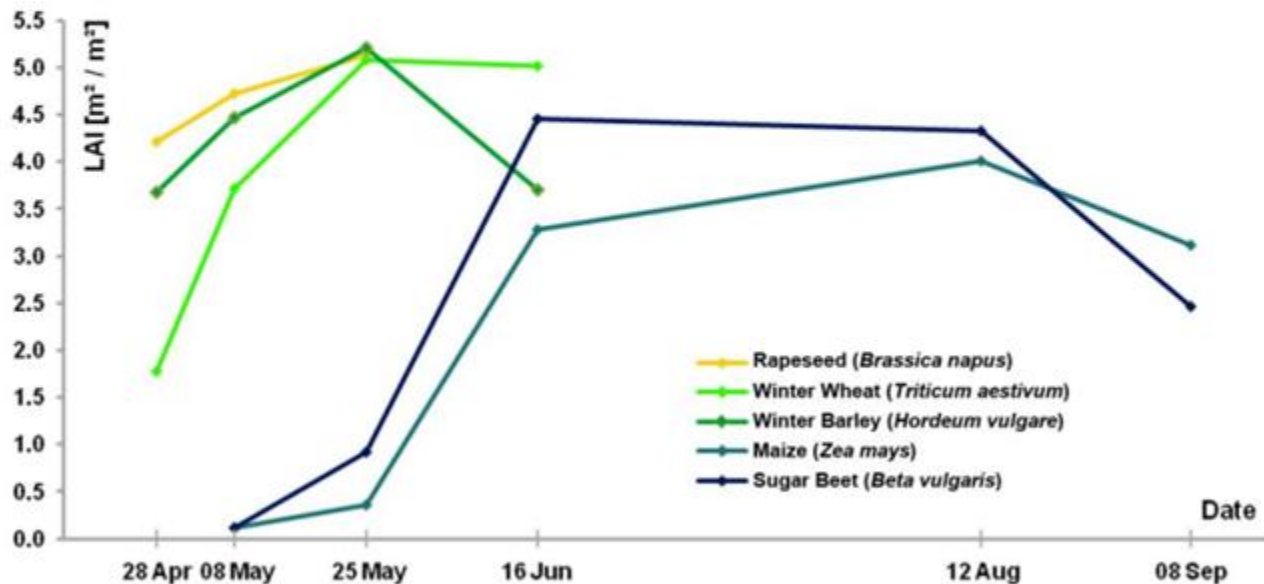


Figure 6. Seasonal development of LAI for the five investigated crops throughout the growing period of 2012, derived from six data acquisitions.

Data

1. Prosail simulation of AVIS-3

2. strategies. The airborne imaging spectrometer AVIS-3 (Airborne Visible and Near Infrared Spectrometer, LMU, Munich, Germany), developed at the Department of Geography of the Ludwig Maximilian University (LMU) [19], was used to perform four imaging flights during the course of the vegetation period of 2012 over a 12 km² large test site in Southern Germany (Neusling, Lower Bavaria, central coordinates: 48.69° N, 12.87° E). The seasonal campaign was complemented by two additional acquisitions from the airborne sensor HySpex, which is operated by the German Aerospace Center (DLR) [20].

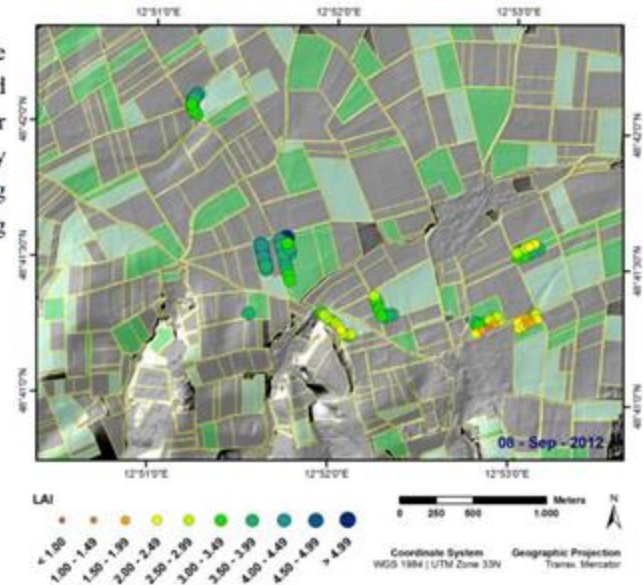
In order to validate the methods developed for the retrieval of biophysical parameters, an extensive field campaign was carried out alongside the airborne data acquisitions, resulting in more than 330 valid LAI measurements of five different crops. These represent the major crops cultivated in the area (winter wheat, winter barley, rapeseed, maize, sugar beet). The LAI measurements were conducted non-destructively using LAI-2000 plant canopy analyzers (Li-Cor, Lincoln, NE, USA), applying a diagonal sampling pattern (two reference and eight canopy measurements) within elementary sampling units corresponding to the geometric resolution of the airborne data.

1. Prosail simulation of Enmap

2. AVIS-3 simulation of Enmap

Table 1. Airborne data acquisitions over the Neusling test site.

Acquisition Date	Sensor	Sun Zenith (°)	Sun Azimuth (°)
28 April	AVIS-3	42	132
8 May	HySpex	45	115
25 May	AVIS-3	39	236
16 June	AVIS-3	28	146
12 August	HySpex	42	133
8 September	AVIS-3	45	155



Prosail inversion of EnMAP - ground truth?

In order to evaluate the capacity of the analysis method for the retrieval of LAI from future EnMAP data, the LUT inversion was adapted and repeated on the simulated EnMAP data, based on the identical setting as it had been used for the airborne data. The application of the inversion method to the simulated EnMAP data requires validation as well. This, however, is not easily done based on *in-situ* measurements, since ground measurements naturally only are representative for the spatial resolution for which they were collected. In our case, the LAI data was sampled at a diagonal sampling pattern within ESUs of 4 by 4 m and thus correspond to the 4 m scale of the airborne data. EnMAP, however, will operate at a geometric resolution of 30 m, making it very hard to acquire statistically significant amounts of overpass-parallel *in-situ* measurements for ESUs of that considerable spatial extent. Consequently, another approach was chosen, which uses the results of the parameter retrieval based on the airborne image data. Since the estimation accuracy on the 4 m scale of the airborne acquisitions was proved to be acceptable by validation against *in-situ* data, the validated output images were scaled up to the spatial resolution of 30 m, thus generating a validated spatial LAI map at 30 m resolution. This validated map then was consulted as reference for the LAI map that was originally retrieved from the simulated EnMAP data at 30 m resolution. The acquisition of the second flight on 8 May 2012 was used for the comparison. In Figure 7, the LAI image retrieved from the simulated EnMAP scene and the upscaled airborne LAI map are presented.

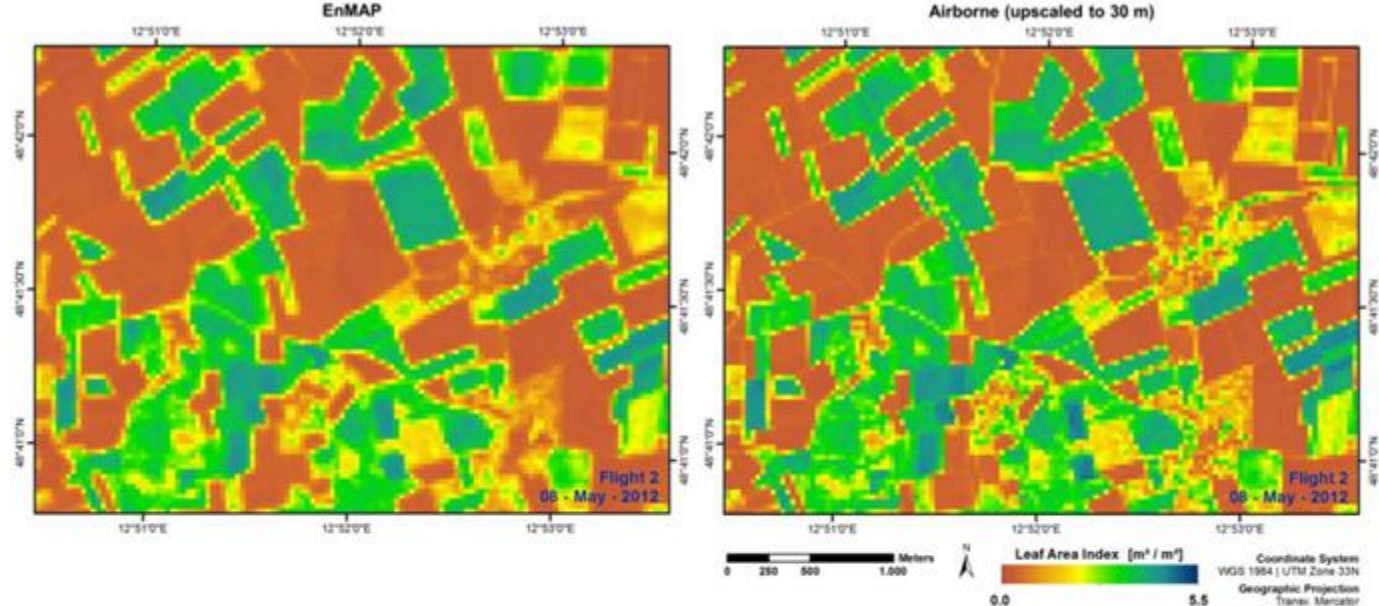


Figure 7. Comparison of estimated LAI (8 May 2012), which was derived by the adapted LUT algorithm from simulated EnMAP data (**Left**) and upscaled (from 4–30 m) LAI estimation based on the 4 m airborne data (**Right**).

The visual interpretation of Figure 7 shows that the estimations of LAI appear to have led to very similar results in both maps. To further assess the consistency between airborne and EnMAP retrieval, an uncertainty map of both scales is presented in Figure 8, giving the standard deviation of all considered estimated LAI values ($n = 350$) per pixel before averaging. The maps, one for the airborne and one for the EnMAP-scale retrieval, give a spatial measure of how definite the resulting LAI value was found

among the simulated spectra that were selected by the inversion routine. By comparing Figures 7 and 8, it can be observed that high LAI values are generally associated with higher uncertainty. The highest levels of uncertainty are observed for the forested areas in the South of the test area. This can to some degree be traced to the fact that the parameters included in the LUT were not designed to include characteristics of forested areas, because forests were not targeted in this study. For both scales, the standard deviation among the 350 best fits is roughly 1 LAI unit. However, it also can be deduced that the model uncertainty on average increases by 3% when going from the airborne (Figure 8, right) to the satellite borne scale (Figure 8, left).

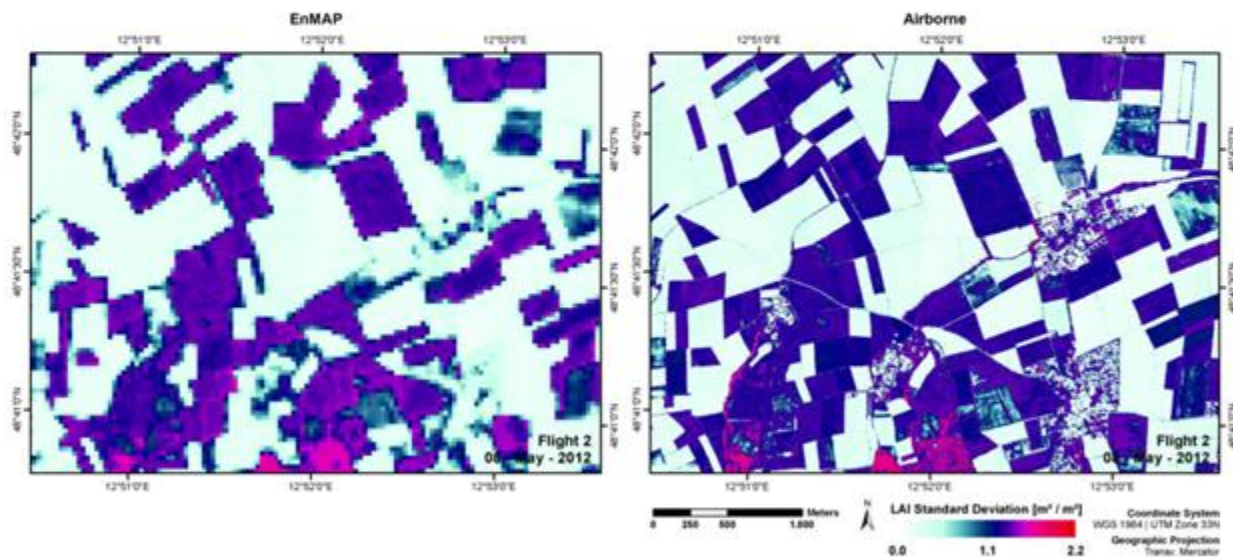


Figure 8. Standard deviation of all considered estimated LAI values ($n = 350$) before averaging, giving a spatial measure of model uncertainty for the retrieval of LAI from simulated EnMAP data (Left) and from airborne data (Right).

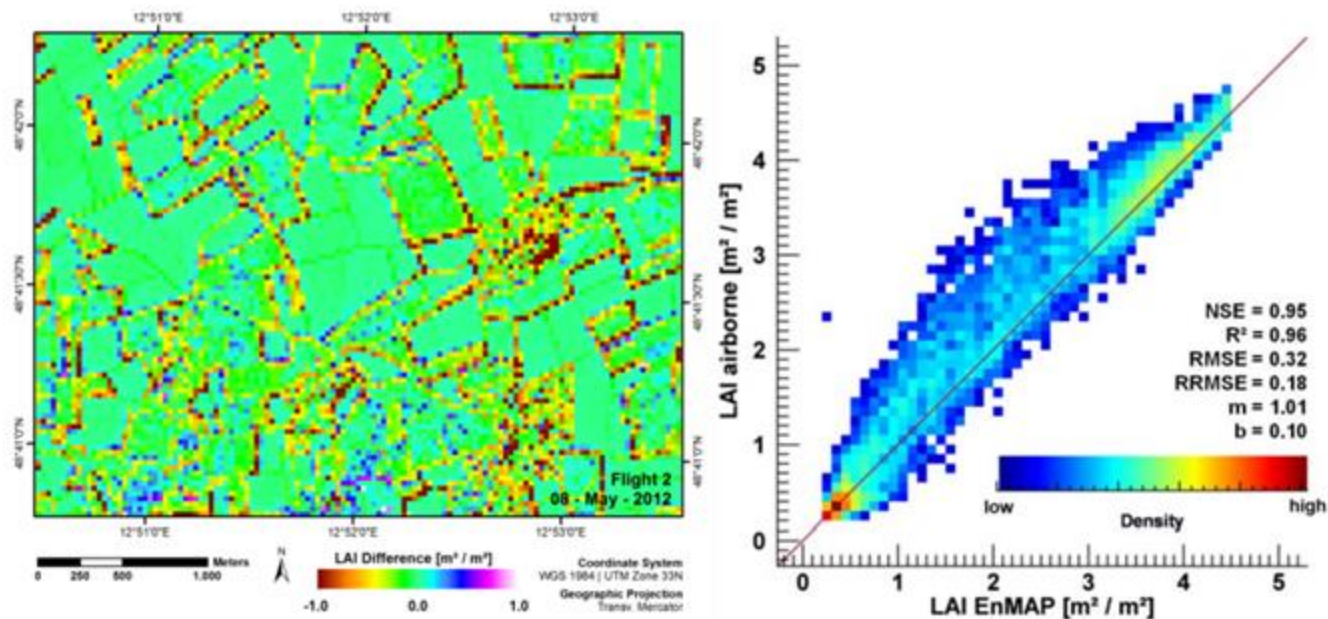


Figure 9. Difference map calculated from the LAI estimations based on simulated EnMAP and upscaled original airborne data (**Left**) and density plot showing a pixel-wise comparison of both spatial data sets (**Right**).

In order to examine local deviations and to determine whether they follow a spatial pattern, a map was calculated showing the difference between the simulated EnMAP and the upscaled airborne estimation (Figure 9, left). Further, the agreement between both spatial data sets was calculated by confronting each pixel of the LAI-EnMAP map to the corresponding one of the airborne scale LAI map (Figure 9, right).



Contents lists available at [ScienceDirect](#)

Int J Appl Earth Obs Geoinformation

journal homepage: www.elsevier.com/locate/jag

Estimation of leaf area index using PROSAIL based LUT inversion, MLRA-GPR and empirical models: Case study of tropical deciduous forest plantation, North India

Sanjiv K. Sinha^a, Hitendra Padalia^{a,*}, Anindita Dasgupta^a, Jochem Verrelst^b, Juan Pablo Rivera^c

^a Indian Institute of Remote Sensing, Indian Space Research Organisation (ISRO), 4-Kalidas Road, Dehradun, 248001, Uttarakhand, India

^b Image Processing Laboratory (IPL), Parc Científic, Universitat de València, 46980 Paterna, València, Spain

^c Conacyt-UAN-CENIT2 Centro Nayarita de Innovación y transferencia de tecnología, Calle 3 esquina con Av. 9 /n colonia Ciudad Industrial, 63173 Tepic, Nayarit, Mexico

[HTML] Estimation of leaf area index using PROSAIL based LUT inversion, MLRA-GPR and empirical models: Case study of tropical deciduous forest plantation ...

[SK Sinha](#), [H Padalia](#), [A Dasgupta](#), [J Verrelst](#)... - International Journal of ..., 2020 - Elsevier

Forests play a vital role in biological cycles and environmental regulation. To understand the key processes of forest canopies (eg. photosynthesis, respiration and transpiration), reliable and accurate information on spatial variability of Leaf Area Index (LAI), and its seasonal dynamics is essential. In the present study, we assessed the performance of biophysical parameter (LAI) retrieval methods viz. Look-Up Table (LUT)-inversion, MLRA-GPR (Machine Learning Regression Algorithm-Gaussian Processes Regression) and empirical models, for ...

☆ Save Cite Cited by 59 Related articles All 6 versions Web of Science: 46

Questions?